School of Science

SCIE896 Dissertation

Phosphate Sensors Formed by the Self-Assembly of Fluorescent Probes

Olivia Matich

ID: 17983516

A dissertation submitted in partial fulfilment of the requirements for the degree of Bachelor of Advanced Science (Honours)

Auckland University of Technology

February 2022

Abstract

The purpose of this research is to design and synthesise a self-assembled receptor/sensor system capable of detecting phosphate oxoanions. The development of artificial sensors which can selectively detect phosphates (such as ATP and PPi) has exciting bioanalytical applications as phosphorylated compounds are important mediators of numerous biochemical processes. Our designed sensor consists of zinc-dipicolylamine units that have previously been shown to detect phosphate functional groups. The introduction of a long hydrophobic tail is used to bring two zinc-dipicolylamine units close together, driving the self-assembly of a supramolecular complex that is able to bind phosphates. By combining this complex with the colorimetric dye bromopyrogallol red, we were able to construct an indicator displacement assay (IDA) that has different selectivities for a range of inorganic phosphates. With this study, we demonstrate that self-assembly can be an exciting new approach for constructing artificial sensors.

Table of Contents

Abbreviations

δ	Chemical shift
°C	Degrees Celsius
µM	Micromolar
ADP	Adenosine diphosphate
AMP	Adenosine monophosphate
ATP	Adenosine triphosphate
BPR	Bromopyrogallol red
cAMP	Cyclic adenosine monophosphate
COSY	Correlated spectroscopy
d	Doublet
DCM	Dichloromethane
dd	Doublet of doublets
ddd	Doublet of doublet of doublets
DIPEA	*N,N*-Diisopropylethylamine
DMF	*N,N*-Dimethylformamide
DMP	Dimethyl phosphate
DNA	Deoxyribonucleic acid
EDC-HCl	1-(3-dimethylaminopropyl)-3-ethylcarbodiimide hydrochloride
et al.	and others
EtOH	Ethanol
eq.	Equivalents
g	Grams
HEPES	2-[4-(2-hydroxyethyl)piperazin-1-yl]ethanesulfonic acid
HMBC	Heteronuclear multiple bond correlation
HOBt	Hydroxybenzotriazole
HPNPP	2-hydroxypropyl-4-nitrophenol phosphate
HRMS	High resolution mass spectrometry

HSQC	Heteronuclear single quantum coherence
Hz	Hertz
IDA	Indicator displacement assay
IR	Infrared
J	Coupling constant
m	Multiplet
M	Molar
MeCN	Acetonitrile
MeOH	Methanol
mL	Millilitre
mM	Millimolar
mmol	Millimolar
NEt_3	Triethylamine
nm	Nanometers
NMR	Nuclear magnetic resonance
PPi	Pyrophosphate
ppm	Parts per million
PV	Pyrocatechol violet
quat	Quaternary
R	Unspecified alkyl group
RNA	Ribonucleic acid
s	Singlet
t	Triplet
TACN	1,4,7-triazacyclononane
td	Triplet of doublets
TLC	Thin-layer chromatography
UV	Ultraviolet
UV-vis	Ultraviolet-visible

List of Figures

Attestation of Authorship

I hereby declare that this submission is my own work and that, to the best of my knowledge and belief, it contains no material previously published or written by another person (expect where explicitly defined in the acknowledgements), nor material which to a substantial extent has been submitted for the award of any other degree or diploma of a university or other institution of higher learning.

Olivia Matich

19th February 2022

Acknowledgements

I would like to thank my supervisor, Dr. Jack Chen, for all his help and support during this research project. His availability to answer my constant questions was much appreciated and allowed me to develop my research skills both in and out of the laboratory. The knowledge and confidence I have gained working in Jack's research group has encouraged me to continue with research in my future studies.

Thank you to Chloe and Mohinder for their help and support in the lab. Their insight into organic synthesis and UV-vis spectroscopy proved valuable in assisting me with my research. They were always available to teach me new skills or answer my questions which helped me throughout this project.

Thank you to my friends and family for their love and support through all the hard times and uncertainty that came along with completing this project.

Chapter 1: Introduction

1.1 Receptors

The design of artificial receptors which can selectively recognise different ionic species has become a large area of interest for chemists in recent years. These types of sensors have important biological and environmental applications. For example the monitoring of metabolic and bioenergetic processes, and the detection of pollutants in the environment.[1, 2]

Metal cations such as sodium, potassium, calcium, copper and zinc all have a vital biological role.[2] In contrast lead, cadmium and mercury cations are toxic heavy metals and can cause serious health and environmental issues, thus it is crucial we have a way to detect these in the presence of other ionic species.[2] Biologically important anions such as pyrophosphate (PPi) and adenosine triphosphate (ATP) are involved in most transport and recognition processes in the body.[3] DNA polymerisation involves the hydrolysis of ATP to release PPi.[1] PPi is then involved in the biosynthesis of cyclic adenosine monophosphate (cAMP), an important secondary messenger for regulating the activity of many different hormones.[3, 4] Therefore the ability to selectively detect one type of anionic phosphate in the presence of another has great applications in bioanalytic investigations.

The ability to selectively recognise one ion over another is a key factor for artificial receptors. A receptors target ion will exist amongst other similar species, for example PPi existing in the body alongside other phosphate oxoanions such as ATP and adenosine diphosphate (ADP). Similar species could potentially bind to the receptor giving a false positive. Therefore, the receptor much be able to select the desired species from a sample containing many analytes to ensure that the signal seen is due to the analyte of interest.

Indicator displacement assays (IDAs) are a technique employed to assess the sensing ability of both colourimetric and fluorescent sensors. Initially an indicator reversibly binds to the sensor, then with the addition of a competitive analyte the indicator is displaced as the analyte binds the receptor, giving a signal.[5] Figure 1 gives a schematic

representation of this process. The important factor of these assays is that the affinity of the indicator and sensor is comparable to the affinity between the analyte and sensor.[5] IDAs are an advantageous technique to analyse sensing as they don't require the indicator to be covalently bound to the sensor.[5] Therefore, several different indicators can be employed for the same receptor. IDAs can use either colourimetric or fluorescent dyes. Colourimetric dyes change colour depending on whether they are bound to the sensor or not. This allows for detection with the naked eye, though it is also measured using UV-vis spectroscopy. Fluorescent dyes binding is detected by measuring the change in emission of the system. In general, this technique is more sensitive as fluorescent spectrometers can measure emissions from concentrations much smaller than that for absorbance measurements.[5]

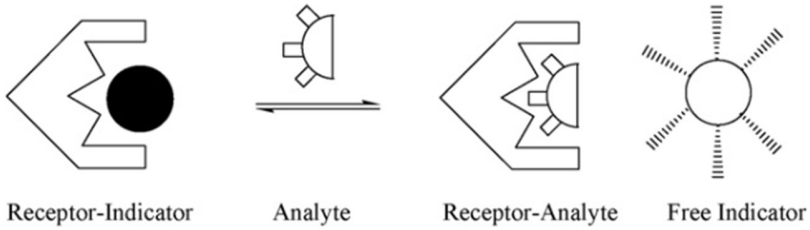

Figure 1: Schematic representation of IDAs. Reprinted with permission from ref. 5. Copyright (2006) Elsevier B. V.

Colourimetric sensors and fluorescent chemosensors are two types of sensors scientists have designed to detect important ionic species.

1.2 Colourimetric Sensors

Figure 2, shows structures of previously synthesised colourimetric sensors for selectively binding phosphates. All of these structures utilise a dipicolylamine group to bind zinc (II) ions. These zinc ions can then bind the catecholate groups of different chromophores, resulting in a colour change which can be monitored spectroscopically. The sensing ability of these compounds was determined using colourimetric IDAs. Here

the chromophore bound to the zinc ion can be displaced in the presence of an analyte.[6] For sensors **1-9** chromophores **10-12** were used in these IDAs. The analytes used were phosphate anions PPi, ATP and ADP which can all bind the zinc ions.

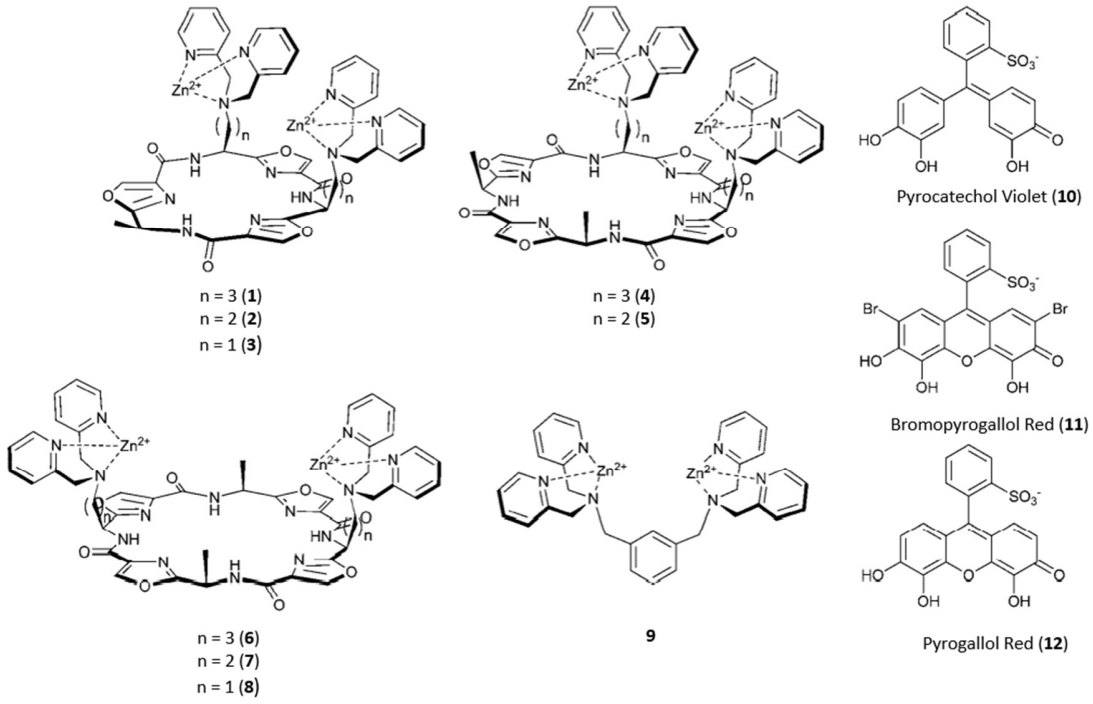

Figure 2: Structures of sensors consisting of dipicolylamine groups and chromophores with catecholate groups, used for IDAs. Reprinted with permission from ref. 1. Copyright (2013) The Royal Society of Chemistry.

Prior to testing the performance of the IDAs, the binding of the chosen chromophore was monitored spectroscopically. In Figure 3a the binding of pyrocatechol violet (PV) **10** to sensor **6** was monitored, with increasing concentrations of **6**. Here they saw the absorption band at 640 nm increase while the band at 444 nm decreased, until saturation is reached with the formation of 1:1 complexes.[1] Jolliffe and co-workers then monitored the absorbance of this 1:1 (sensor **6**: PV) complex when PPi is added at

increasing concentrations. PPi successfully displaced PV from the sensor, seen by the increase in the band at 444 nm and decrease of the band at 640 nm, in Figure 3b.[1]

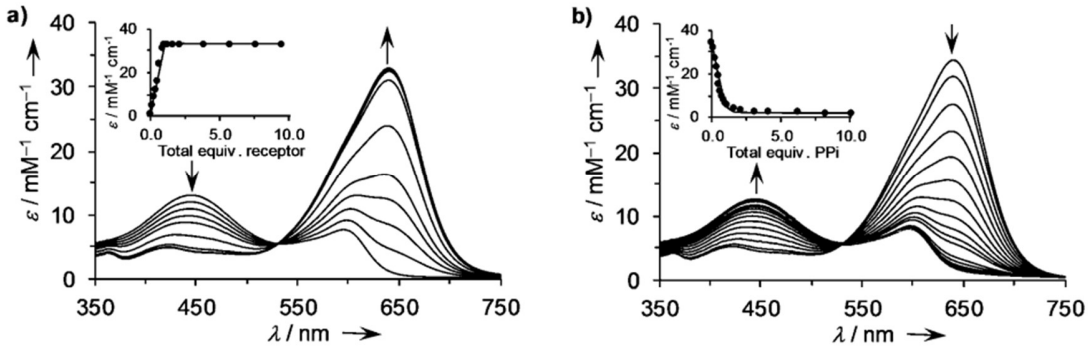

Figure 3: Changes in absorbance when PV is added to varying concentrations of sensor **6** (a) and when PPi is added in varying concentration to the PV: sensor **6** complex (b). Reprinted with permission from ref. 1. Copyright (2013) The Royal Society of Chemistry.

The next step in Jolliffe and co-workers' investigation was to determine whether their sensors was selective for PPi over other phosphates (ATP, ADP, AMP, c-AMP, phosphothreonine, phosphoserine, phosphotyrosine, HPO_4^{2-}, and citrate). Ideally sensors should be able to selectively detect the desired phosphate in the presence of other species. This ensures that any signal seen in a real-life system is due to the species of interest and not competing ions present. Jolliffe and co-workers' experiments used five equivalents of phosphate to displace PV from the ligand. PPi, ATP, ADP and citrate were able to displace PV from the ligand seen by the colour change from blue to yellow or green.[1] By altering the length of the side chains between the dipicolylamine groups and the cyclic scaffold they were able to alter the selectivity, with shorter side chains resulting in only PPi and ATP displacing PV.[1] Essentially they found that stoichiometries of >1 receptor: 1 indicator provided improved selectivity, along with the choice of indicator.[1]

Overall, this research demonstrated that IDAs can be used to assess colourimetric sensors and that the dipicolylamine group along with zinc ions can successfully and selectively detect phosphates.

1.3 Fluorescent Chemosensors

Fluorescent chemosensors are compounds which consist of a binding site, fluorophore and communication mechanism.[2] The presence of a fluorophore allows sensing to be detected via fluorescence spectroscopy. Fluorescent sensors are much more sensitive than those based on UV absorption.[1] They can detect lower concentrations of ions, making fluorescent sensors a popular choice for chemists.[5] These type of sensors have been around for 150 years and have a wide range of applications in biology, pharmacology and environmental science.[2] Initially fluorescent chemosensors were designed to detect cation species, specifically metals due to their selective binding in water compared with anions or neutral species.[2] Figure 4 shows fluorescent chemosensors (**13** and **14**) designed to detect alkali metal ions, inspired by the first reported fluorescence chemosensor in 1867 by Goppelsröder.[2] These sensors detect cations via coordination interactions.[7]

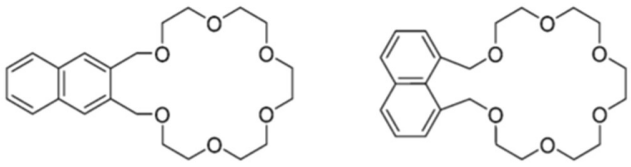

13 **14**

Figure 4: Structure of two cationic fluorescent chemosensors. Adapted with permission from ref. 2. Copyright (2017) The Royal Society of Chemistry.

Nowadays, fluorescent chemosensors have been designed to detect cations, anions, neutrals small molecules and even biomacromolecules such as proteins and DNA.[2]

1.4 Sensors for Phosphate Oxoanions

The development of anion sensors lagged behind that of cation sensors, though this was propelled forward by the important roles that anions play in both biological and industrial processes.[2] In particular phosphate oxoanions are fundamental in biological processes such as energy transduction, signal processing and the storage of genetic information.[3] The phosphate oxoanion PPi is present as a hydrolysis product of ATP, a side product from DNA/RNA polymerase reactions and is used in the biosynthesis of cAMP.[3] Therefore, a lot of research has gone into designing anion sensors that can detect phosphate oxoanions such as PPi, alongside systems that can distinguish between a biologically occurring phosphate oxoanion and inorganic phosphates.[3]

Sensor **15** in Figure 5 was found to be successful at sensing PPi. This was determined using a fluorescent IDA whereby **16** was displaced in the presence of PPi.[8] The structure of this sensor consists of two dipicolylamine groups similar to the colourimetric sensors **1-9** previously mentioned. Once again, this group binds zinc ions which can then bind the catechol group of **16**. This results in a decrease in fluorescence intensity as seen in Figure 6a.[8] When PPi is added to this complex at increasing concentrations, the fluorescence intensity increases as **16** is released from the compound, restoring its fluorescence (Figure 6b).[8]

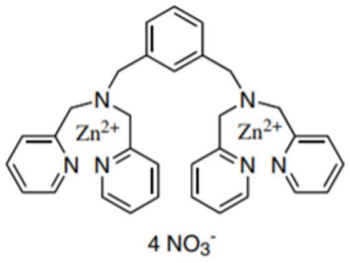

15

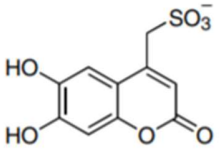

16

Figure 5: Structure of sensor (**15**) and fluorescent indicator (**16**) used for phosphate oxoanion sensing.

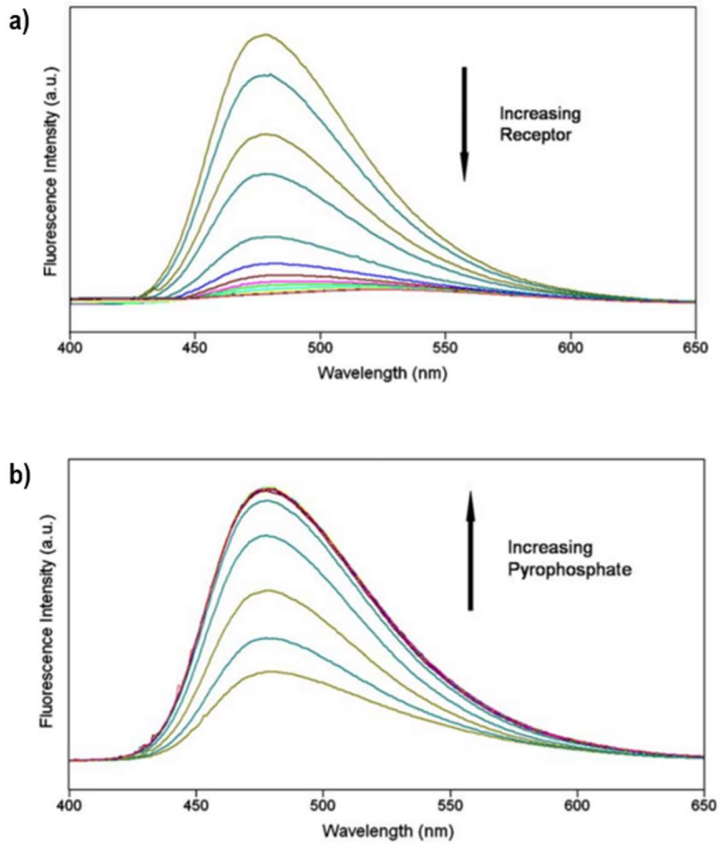

Figure 6: Fluorescence emission spectra of sensor **15** with increasing concentration of fluorescent dye **16** (a) and with increasing concentration of PPi with 1:1 mixture of sensor **15** and **16** (b). Adapted with permission from ref. 8. Copyright (2004) Tetrahedron Letters.

Dipicolylamine has been employed by many research groups in the design of their phosphate oxoanion chemosensors. These functional groups are particularly selective for phosphate oxoanions over other anions.[3] Zinc ions have a strong binding affinity for PPi which allows these groups to not only sense PPi but be selective for this in the presence of other phosphate oxoanions.[2] Sensor **17** (shown in Figure 7) is a naphthalene derivative which can detect PPi in water at nanomolecular concentrations.[2] It can also detect less than one equivalent of PPi when present in a 50- to 250- fold

excess of ATP. This was the first reported example of a metal complex capable of differentiating between different phosphate oxoanions (PPi and ATP).[2]

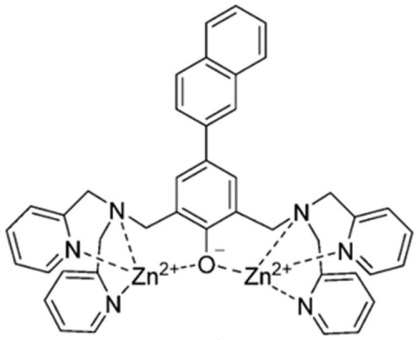

17

Figure 7: Structure of the first metal complex chemosensor which can differentiate between PPi and ATP.

One way by which researchers have designed sensors that are selective for different phosphate oxoanions is by attaching dipicolylamine ligands onto a molecular scaffold.[3] The idea here is that the distance between the two zinc dipicolylamine sites can be altered to control the selectivity, as phosphate oxoanions have one or two oxygen atoms bound to each metal centre.[3] Figure 8 shows some of the receptors designed with a molecular scaffold for selectivity. The activity of these sensors was determined using IDAs and then by the use of analogues whereby a fluorophore (in this case a coumarin) was attached. This would result in a similar change in fluorescence as an IDA without the need for the phosphate oxoanion to displace the fluorophore – as it is incorporated into the molecule. Overall they found that by varying the positions of the zinc dipicolylamine groups, along with varying the R groups, they could alter the selectivity of the sensor, with it discriminating PPi from other phosphate oxoanions such as ATP and ADP.[3]

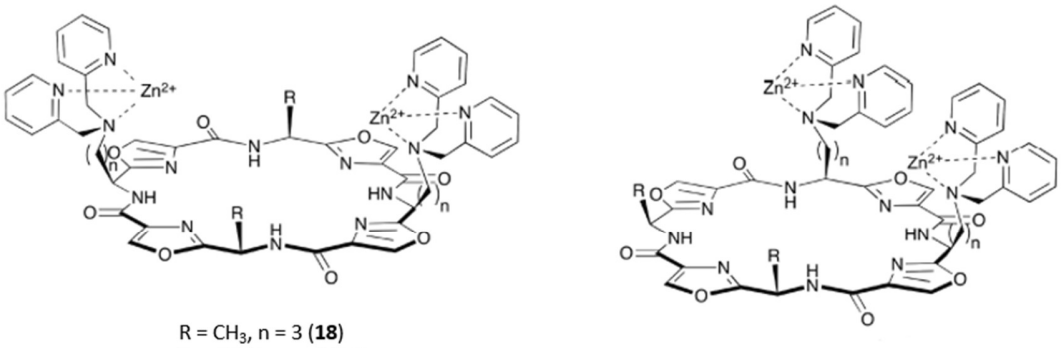

Figure 8: Molecular scaffold structures functionalised with dipicolylamine groups in different positions to alter the selectivity for different phosphate oxoanions. Adapted with permission from ref. 3. Copyright (2017) American Chemical Society.

1.5 Self-assembly

The ability for molecules to self-assemble offers great potential in a number of different research areas. Nanotechnology, a field of great interest in recent years, involves the spontaneous assembly of molecules into nanoparticles, nanotubes and nanorods. All of these structures can then be used for a wide variety of applications in the medical and textile industries.[9, 10] Currently, scientists are using self-assembly to design supramolecular catalysts and artificial sensors.[11] The idea for these is the individual units will assemble under certain conditions to form either a catalyst or a sensor. The assembled version should have an increased activity compared with the disassembled molecules. The main advantage of designing self-assembled systems is the modularity and flexibility of design, especially when compared to systems formed by attachment onto molecular scaffolds or onto dendrimers (Figure 9).

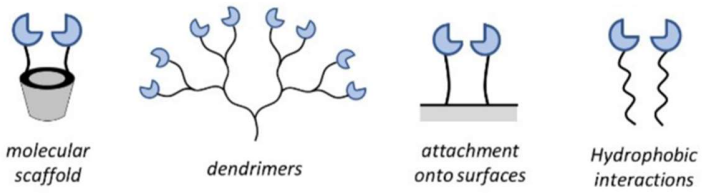

Figure 9: Comparison of different types of systems. Reprinted with permission from ref. 12. Copyright (2021) Advanced Synthesis and Catalysts.

Self-assembled systems can be easily modified without the need for tricky synthesis. Here different ligand combinations, consisting of a variety of functional groups, can be rapidly screened to find the ideal combination. This allows for rapid optimisation and discovery compared with non-self-assembled systems which require total synthesis for any changes to the system.

1.6 Previous Work in the Research Group

Previously our research group has shown that amphiphilic ligands can self-assemble to form vesicles with catalytic pockets on the surface.[11, 13] The aim of the previous research was to design molecules which could self-assemble to form cooperative catalysts capable of breaking down 2-hydroxypropyl-4-nitrophenol phosphate (HPNPP). This requires two catalytic head groups to work together (cooperatively) to cleave the substrate.[11] It was thought that when the molecules formed vesicles that the rate of catalysis would increase as these catalytic head groups would be close together on the surface of these vesicle structures. We designed several different molecules, shown below in Figure 10, using both guanidine **27** and 1,4,7-triazacyclononane (TACN) **28** catalytic head groups, and 16 carbon alkyl chain hydrophobic tails.

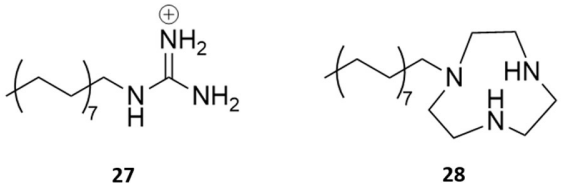

27 28

Figure 10: Guanidine and TACN catalytic amphiphiles

To demonstrate the ability of these molecules to self-assemble, we compared the catalytic activity of these long chain (C_{16}) amphiphilic catalysts with that of short chain (C_4) amphiphilic catalysts. The systems absorbance at 410 nm was used to investigate catalysis as the cleavage of HPNPP produces cyclic phosphate and p-nitrophenolate which is yellow in colour and can be measured spectroscopically. The rate of reaction was then calculated and plotted against increasing concentrations of catalyst, as seen in Figure 11. C_{16}-guanidinium was found to have much greater catalytic activity than C_4 guanidinium.[11]

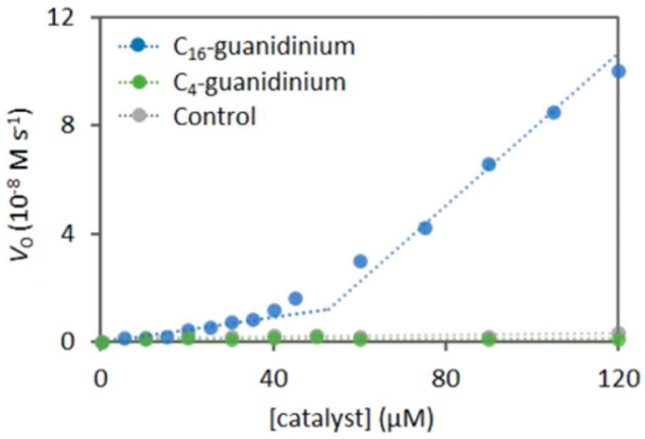

Figure 11: Initial rates of catalysis with increasing concentrations of C_{16}-guanidine and C_4-guanidine. Reprinted with permission from ref. 11. Copyright (2020) American Chemical Society.

Our research group also investigated using different ratios of guanidine **27** and TACN **28** amphiphiles to form different catalytic systems. The modular nature of these self-assembled systems allows for easy modification by changing the concentration of each catalyst present. They found that the particular ratio of 1:3 TACN **28** to guanidine **27** had the greatest catalytic activity.[11]

1.7 Aim of Project

The aim of this project was to employ the concept of self-assembly to develop anion sensors which can detect and distinguish between different phosphate oxoanions. Using the structure of amphiphilic molecules previously designed by our research group (**27** and **28**), we developed several building blocks and control molecules (**29**-**32**). Our previous work utilised long hydrophobic tailed ligands with different hydrophilic head groups (guanidine and TACN).[11] This allowed the molecules to self-assemble under certain conditions, increasing their catalytic activity.[11] We will design and synthesise amphiphilic ligands for phosphate sensing which utilise the previously discussed dipicolylamine group which have high selectivity for phosphate oxoanions.[14]

First, we will synthesis a ligand consisting of the dipicolylamine head group and a long hydrophobic tail (C_{16}) (**29**). The importance of the self-assembly of this ligand in the formation of the supramolecular sensor will be assessed by comparing it to the control molecule **30**, containing the same binding group but a much shorter tail (C_4). Molecule **30** is not expected to self-assemble under the conditions investigated. We expect to see a difference in the ability for **29** and **30** to sense phosphates as two dipicolylamine units must come together to bind phosphate oxoanions. Therefore, **29** should form a better sensor due to its ability to self-assemble and form a supramolecular structure. Scheme 1 shows the simple one-step synthesis required to make these ligands. These compounds will be characterised by NMR, IR and mass spectrometry. The sensing ability of these molecules will be assessed using UV-vis spectroscopy.

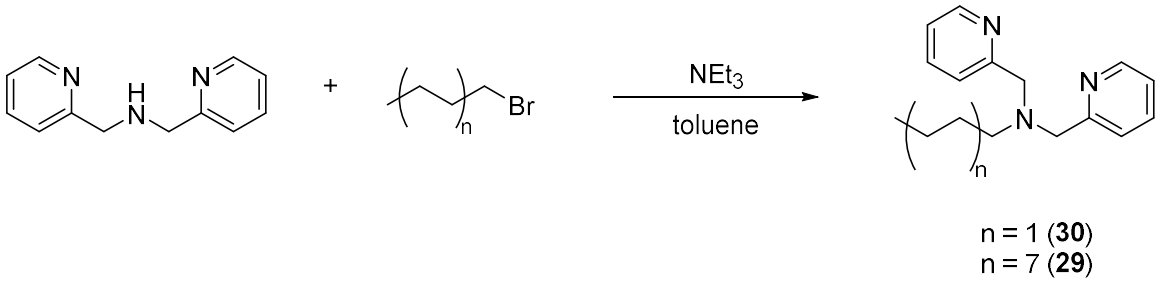

Scheme 1: Synthesis of amphiphilic ligand **29** and control molecule **30**

We also decided to synthesise ligands which incorporated a fluorescent moiety into the structure. We inserted a coumarin in between the dipicolylamine head group and the hydrophobic tail. The idea behind this ligand is that when phosphates are bound, the fluorescence will change, indicating that sensing has occurred. This would allow these molecules to potentially act as fluorescence-based sensors as well as being colorimetric sensors. Once again, a long tail (C_{12}) **31** and short tail (C_4) **32** ligands were synthesised so we can assess the effect of self-assembly. Scheme 2 show the synthetic scheme proposed to synthesise these ligands. These amphiphilic ligands were characterised via NMR, IR and mass spectrometry. Fluorescence and UV-visible spectroscopy were used to assess the sensing abilities of these compounds.

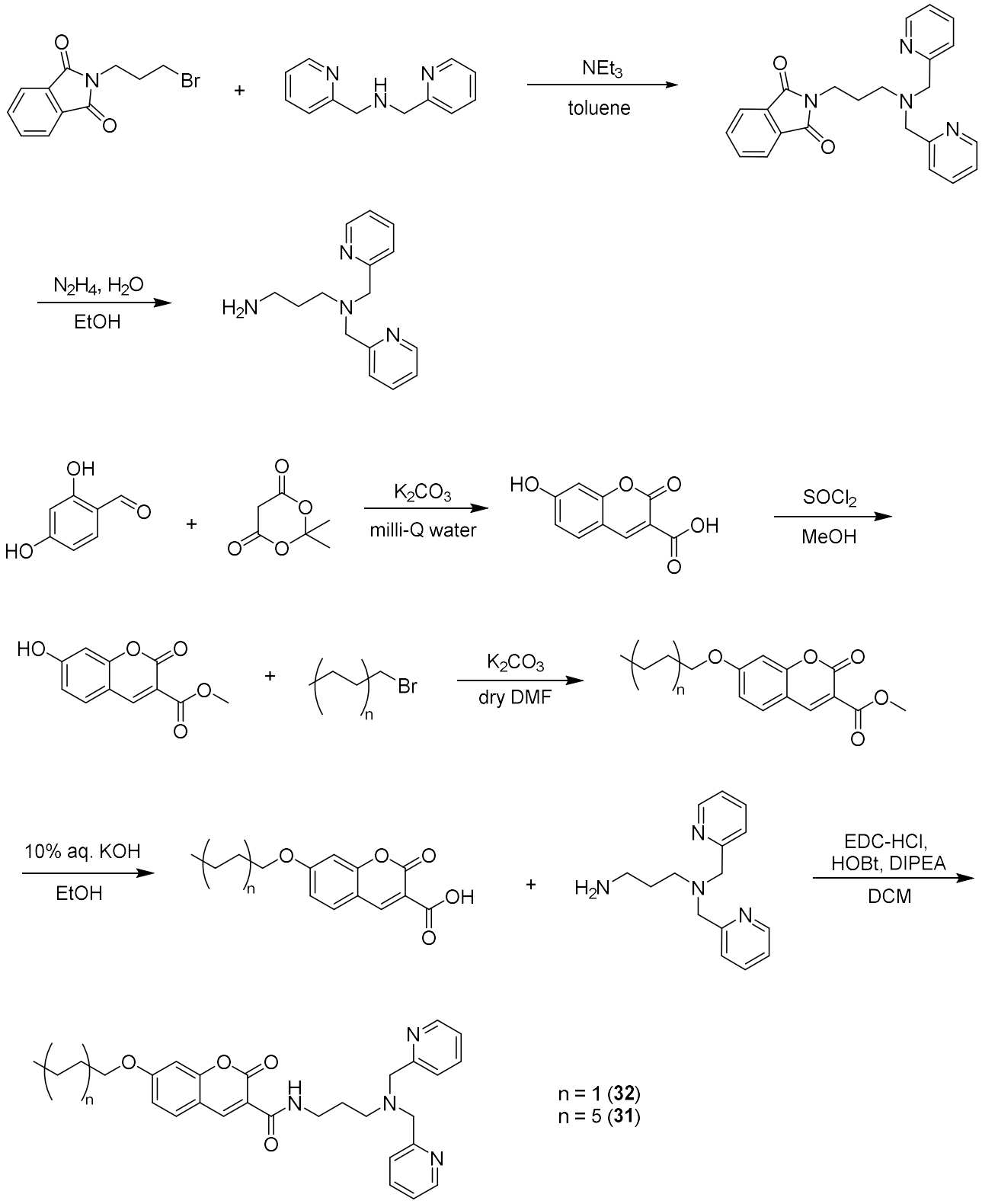

Scheme 2: Synthesis of amphiphilic ligand **31** and control molecule **32**

Chapter 2: Results and Discussion

2.1 Synthesis of Amphiphilic Ligand 29 and Control Molecule 30

Initially, we synthesised amphiphile **29** consisting of a dipicolylamine group and a 16-carbon hydrophobic tail, shown in Scheme 3. This was a relatively simple proposed synthesis consisting of just one step – the nucleophilic substitution of bromine for the dipicolylamine group via an S_N2 mechanism. This step was attempted several times, summarised in Table 1, before we obtained the pure compound. We found the reaction itself to be successful, however the purification proved difficult.

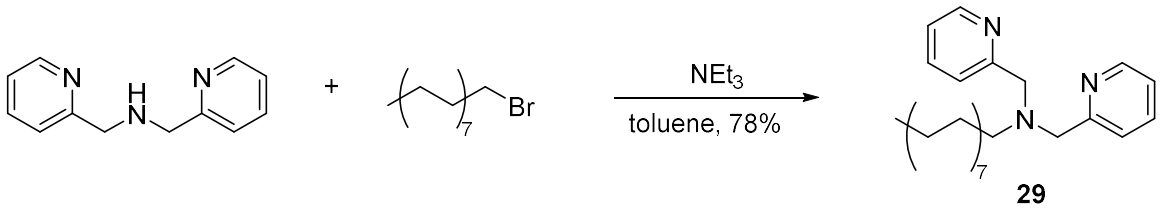

Scheme 3: Synthesis of amphiphile **29**

Table 1: Optimisation table for the synthesis of **29**

Reaction	Dipicolylamine	1-bromohexadecane	Base	Solvent	Pure Product Yield
Attempt 1	1 eq.	1 eq.	3 eq. K_2CO_3	Acetonitrile	0%
Attempt 2	1 eq.	1.2 eq.	3 eq. K_2CO_3	Acetonitrile	1%
Attempt 3	1.2 eq.	1 eq.	3 eq. NEt_3	Toluene	69%

In attempt 1 we tried to purify the product twice via flash chromatography. Initially we used 10% MeOH/$CHCl_3$ + 1% NH_4OH, however this resulted in both spots on the TLC

eluting together. Thinking that this may be due to the polarity of the mobile phase being too high we decreased the polarity to 5% MeOH/$CHCl_3$ + 1% NH_4OH. Once again, the two spots eluted together and NMR analysis showed that the product was present along with a high number of impurities. Attempt 2 had 1-bromohexadecane in excess to ensure that all of the dipicolylamine reacted. Since 1-bromohexadecane is non-polar it should be easier to separate during flash chromatography than dipicolylamine. The reaction appeared to have reached completion after three days, however there was still dipicolylamine present in very small amount (visible on TLC). Flash chromatography was used for purification with 2% MeOH/$CHCl_3$ + 1% NH_4OH, though we did not get any separation. A prep TLC was then used to try to purify the compound. 100 mg of crude material gave 20 mg of product with a slight impurity present. We then ran a second prep TLC on the 20 mg to obtain 5 mg of pure product.

For attempt 3 we decided to use different reagents and different equivalents to see if we could get better conversion of the starting materials to the product. We decided to have the dipicolylamine in excess to see if that would use up all of 1-bromohexadecane as previously we had not managed to react all of the amine. After three days, we did not get complete conversion of starting material to the product though the reaction seemed to have stopped. Flash chromatography was again used for purification. The first column ran used a mobile phase of 4% MeOH/$CHCl_3$. This gave the product with a small impurity so we ran a second column starting with a lower polarity of the mobile phase, 2% MeOH/$CHCl_3$ and increased it to 4% MeOH/$CHCl_3$. This solvent system managed to purify the compound with a yield of 78%. This was a great improvement on the previous two attempts.

To successfully test the self-assembled nature of this ligand we needed to synthesis a control molecule, picolyl ligand **30**. This was synthesised using the method optimised for **29**. Flash chromatography using a gradient of solvents starting with $CHCl_3$ then increasing to 2% MeOH/$CHCl_3$ and then 3% MeOH/$CHCl_3$ furnished the product with a yield of 69%.

2.2 Synthesis of Amphiphilic Ligand 31 and Control Molecule 32

The next step in this process was to synthesise amphiphilic ligand **31** which consists of a fluorescent coumarin moiety. Seven key synthetic steps were used to synthesise ligand **31** summarised in Scheme 4.

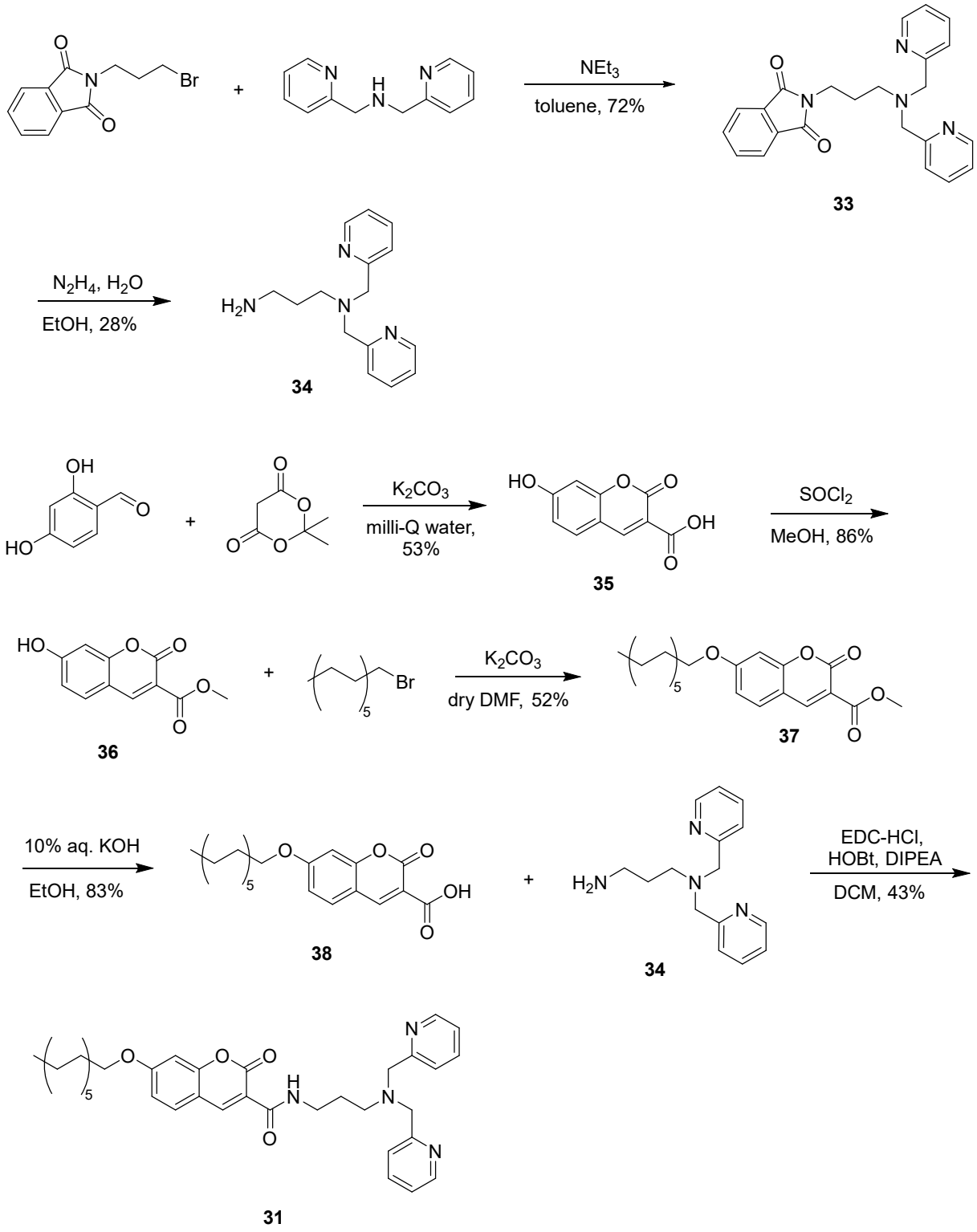

Scheme 4: Synthesis of amphiphilic ligand **31**

The first step involves the nucleophilic substitution of dipicolylamine with N-(3-bromopropyl) phthalimide via an S_N2 mechanism. Previous synthesis of molecules containing a dipicolylamine group (**29** and **30**) had difficulties with purification due to the polarity of this group. Therefore, we decided to try purification via alumina flash chromatography as opposed to the traditional silica. Polar compounds stick strongly to the silica stationary phase and either do not move or become very streaky. We have seen this with our previous silica columns as we get a long band of product resulting in poor separation. Silica is also slightly acidic which means it can protonate the nitrogen of amines giving the compound a positive charge, making it stick to the silica even more. Since the ionic and non-ionic forms of an amine exist in equilibrium, we get a broadened band hindering successful separation. Using an alumina stationary phase as opposed to silica is favourable for purifying amines as it removes several of these issues. Alumina is less polar than silica so our rather polar compounds should not stick as strongly giving better separation. It is also slightly basic in nature so we won't get unwanted protonation of our products. Ultimately this makes alumina the idea stationary phase for amine purification. When synthesising amine **33** we tried both silica and alumina stationary phases to determine whether alumina would make purification easier for our future amine compounds. The silica column gave a yield of 59%. This was a pretty good result; however, the column took a very long time to run due to the amine sticking to the stationary phase. It also took a long time to elute from the column due to the long product band. The alumina column gave a yield of 72%. With a shorter run time and product elution time, alumina proved to be the better method to purify amines. Going forward this was to be our new method for purifying all compounds containing a dipicolylamine group.

The second step involved the liberation of the amine from the phthalimide protecting group to give **34**. The mechanism for this is depicted in Scheme 5. Initially one of the nitrogen atoms in hydrazine undergoes a nucleophilic acyl substitution with one of the phthalimides carbonyl groups. The hydrazine, now attached to the carbonyl, loses a proton to the positively charged nitrogen. The second free amine in hydrazine then undergoes a nucleophilic acyl substitution with the other carbonyl group. This results in

the amine being released. Finally, this amine takes a proton from the positively charged nitrogen in the phthalimide producing the desired amine and phthalhydrazide.

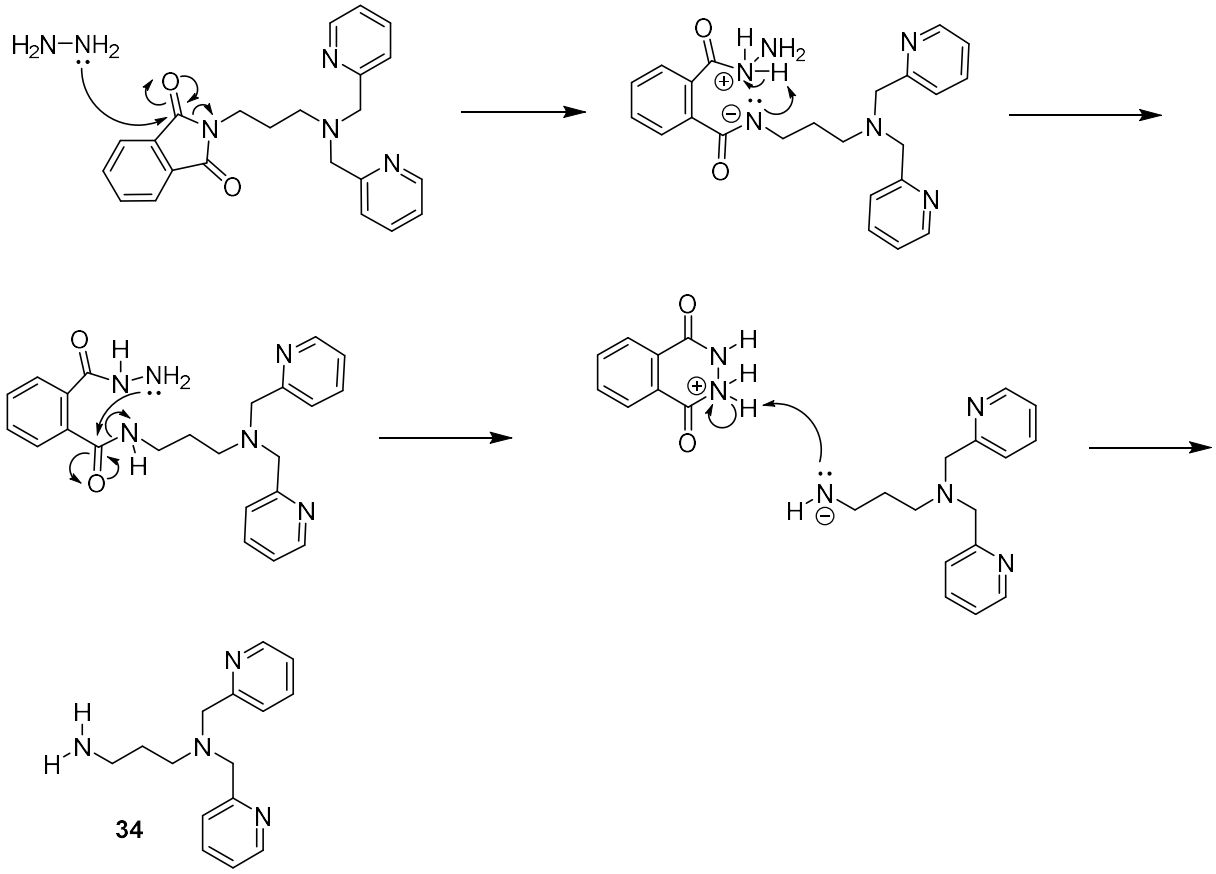

Scheme 5: Amine liberation from phthalimide

Amine **34** is a very polar compound and proved very difficult to purify. This amine was extracted into the aqueous layer to give the almost pure compound. However, alumina chromatography was again used though because this amine is much more polar than the previous compound it was not as successful. The overall process was difficult though we obtained a decent yield of 28%.

Coumarin **35** was then synthesised, with the mechanism shown below in Scheme 6. The first step involves the deprotonation of one of the acidic protons of Meldrum's acid

by K_2CO_3. This forms an enolate. The electrons in the double bond of the enolate can attack the carbonyl functional group present in 4-hydroxysalicyl aldehyde. At the same time, we reform the carbonyl group. This gives a negatively charged oxygen which can pick up a proton. The remaining acidic proton from Meldrum's acid is then deprotonated by the base to form a second enolate. Once again, the carbonyl group is reformed from the enolate, resulting in the loss of OH^- from the compound. This occurs via an E1cB mechanism, whereby the elimination of OH^- is favourable as it occurs from a negatively charged species which becomes neutral as a result. This is a two-step mechanism involving the deprotonation of the alpha proton followed by the loss of OH^-. Next the electrons from the oxygen closest to the carbonyl attack at this position, breaking the bond between the carbonyl carbon and the oxygen in the ring. This now negatively charged oxygen takes the proton from the positively charged oxygen in the newly formed ring. The electrons from the OH can now be used to form a double bond resulting in the breaking of the carbon oxygen bond, losing protonated acetone. This leaves a negatively charged oxygen which can take a proton from protonated acetone to give acetone and the desired coumarin (**35**).

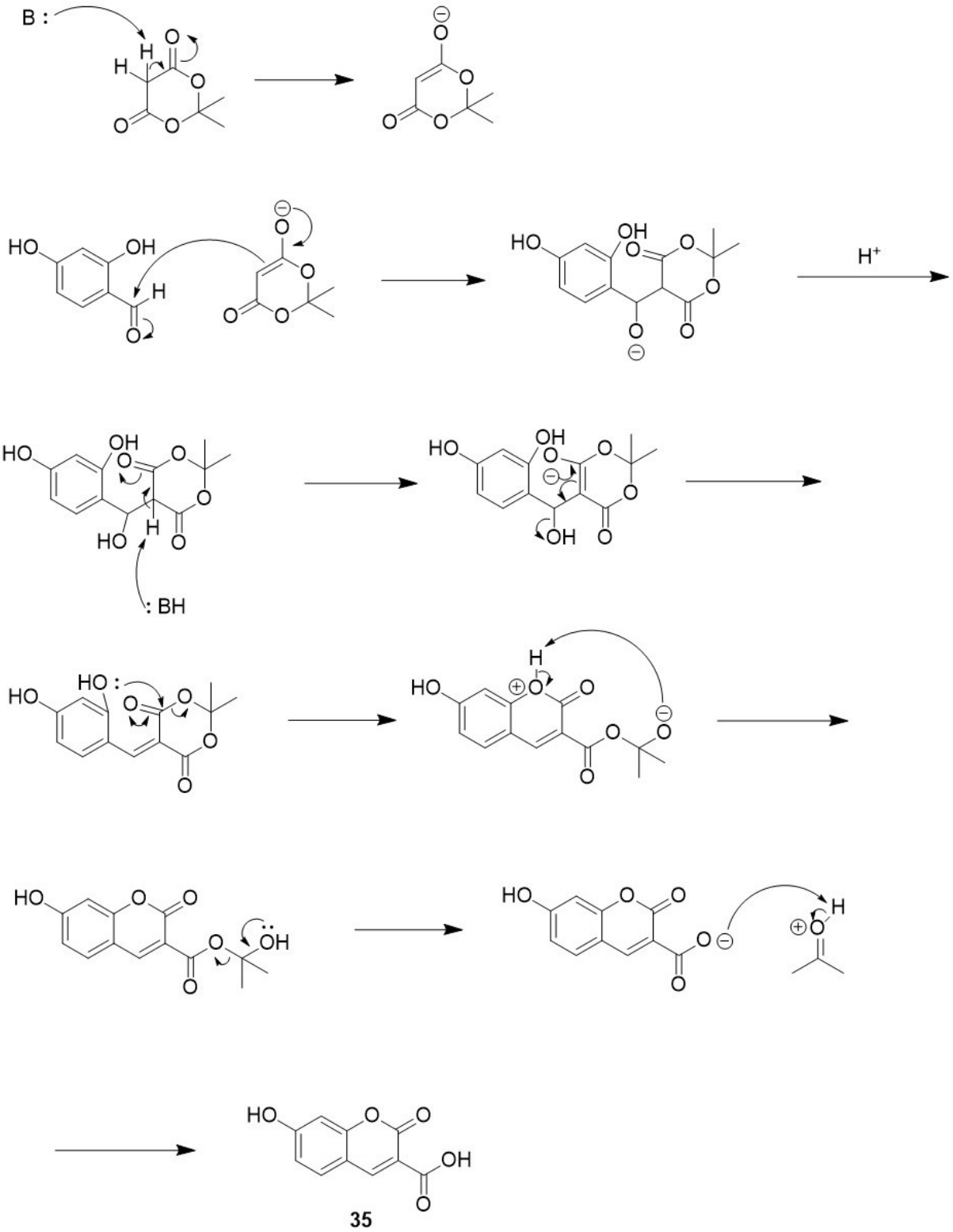

Scheme 6: Mechanism for coumarin formation

Recrystallisation was used to purify coumarin **35**. This resulted in a yield of 20% for the first attempt. In the second attempt, the solution was left overnight to recrystallise, resulting in more of the product coming out of solution and giving a higher yield of 53%.

In the original plan the next step was to react coumarin **35** with amine **34** as shown in Scheme 7. This was to be followed by the alkylation of the coumarin to give the final product (**31**). The issue with this was the product contained several impurities present on the NMR. Throughout this project, we discovered how difficult it is to purify compounds containing the dipicolylamine group. Thus, we decided to redesign our synthesis scheme whereby coumarin **35** would be alkylated prior to reacting with amine **34**. This would eliminate one reaction with a difficult purification and so we should obtain a greater yield of pure products.

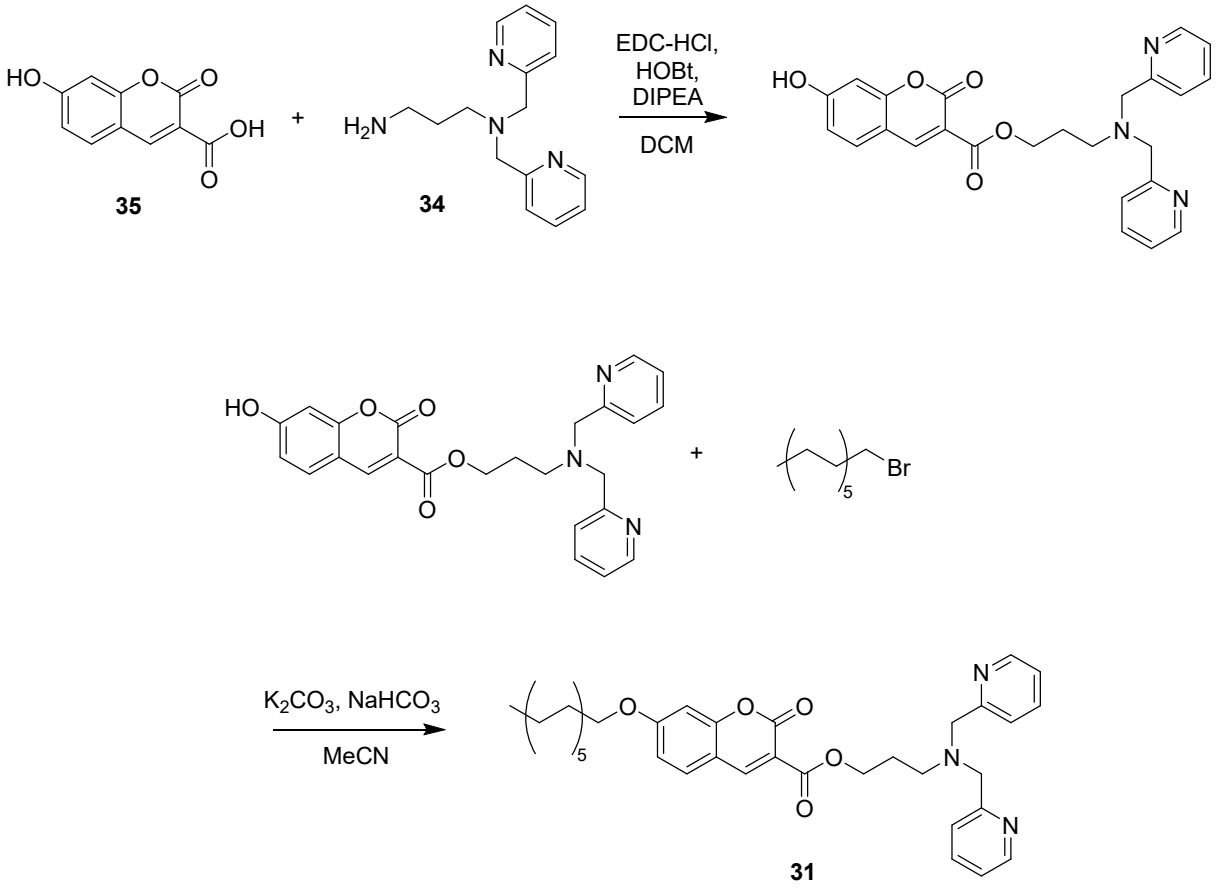

Scheme 7: Final steps from original synthetic scheme

Alkylating coumarin **35** also brought about some challenges. Initially we tried to simply alkylate the alcohol without any protecting group on the carboxylic acid functional group of coumarin **35**. TLC and NMR analysis of the reaction shown in Scheme 8 found that we were getting alkylation at both the alcohol and carboxylic acid positions. Essentially the alcohol is reacting via an S_N2 mechanism, but the reaction conditions also allow the carboxylic acid to undergo ester formation. At the end of this reaction, we had three compounds, singly alkylated coumarin **38** (desired product), double alkylated coumarin and unreacted coumarin **35**.

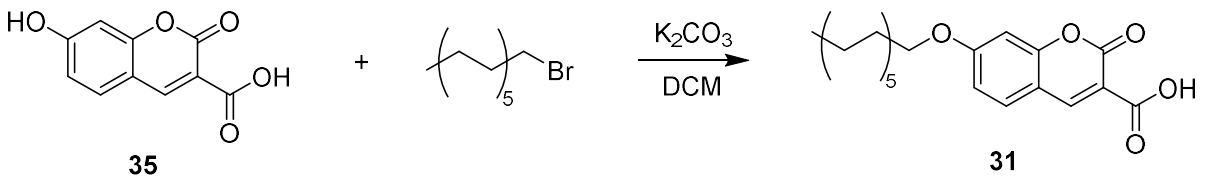

Scheme 8: Alkylation of coumarin **35** without protecting groups.

To prevent unwanted alkylation with our long carbon chain we decided to first protect the carboxylic acid group on coumarin **35** with a methyl group. The mechanism for this esterification reaction is shown below in Scheme 9. This mechanism proceeds in two steps: the formation of the acid chloride followed by the formation of the ester with methanol. Acid chlorides are more reactive than carboxylic acids. This is due to chloride (Cl^-) being a much better leaving group than hydroxide (OH^-). Carboxylic acids can easily be converted to acid chlorides using a chlorinating agent such as $SOCl_2$.[15] The lone pair of electrons from the oxygen move allowing the electrons in the carbonyl group to attack the sulphur of thionyl chloride resulting in the chlorine leaving as an anion. The chloride anion can then attack the carbon in the newly formed double bond. The electrons in the double bond move onto the positively charged oxygen atom. Another chloride anion can deprotonate the OH, resulting in electron movement to form SO_2 and kick out the second chlorine to form HCl. The formation of both of these gases is what drives the first part of this reaction to form the acid chloride. The increased reactivity of the acid chloride functional group allow it to react with an alcohol (in this case methanol)

to form an ester. The electrons on the oxygen of methanol attack the carbonyl of the acid chloride. The electrons from the oxygen then reform the carbonyl resulting in the chloride being kicked out. This gives the desired ester (coumarin **36**).

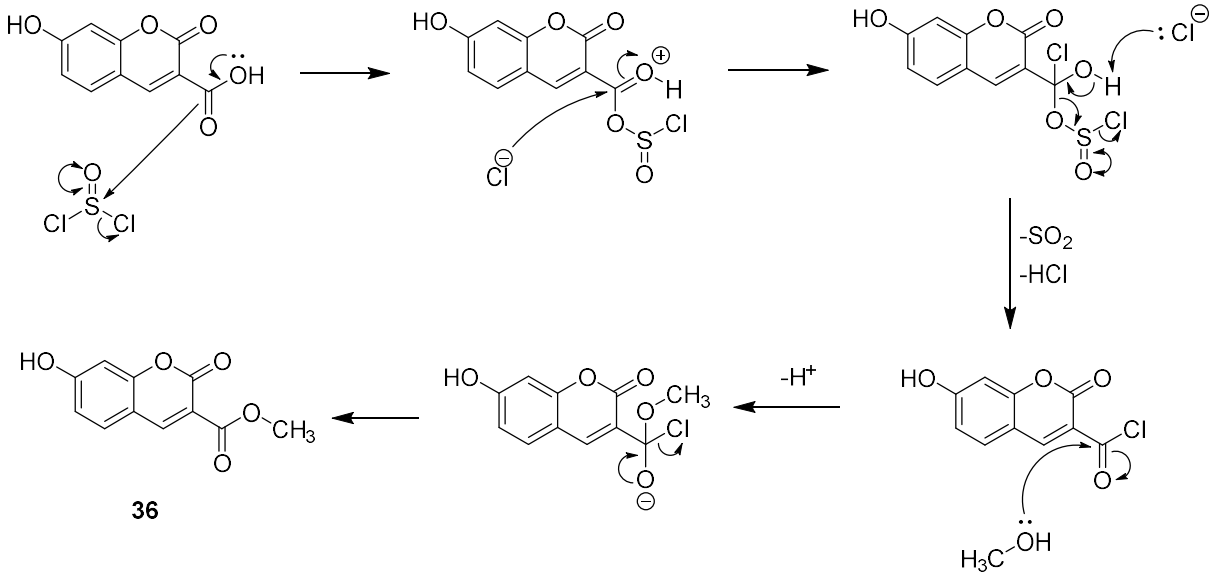

Scheme 9: Esterification mechanism

Now we can alkylate just the desired alcohol. This occurs via a Williamson ether synthesis, depicted in Scheme 10. The reaction is named after Alexander Williamson who first discover it in 1850.[16] This is essentially an S_N2 mechanism for ether formation. Here a base such as K_2CO_3 deprotonates the alcohol to give negatively charged oxygen. The electrons on the oxygen attack the electrophilic carbon on 1-bromododecane. The bromine leaves and this forms KBr and we get the final product, coumarin **37**.

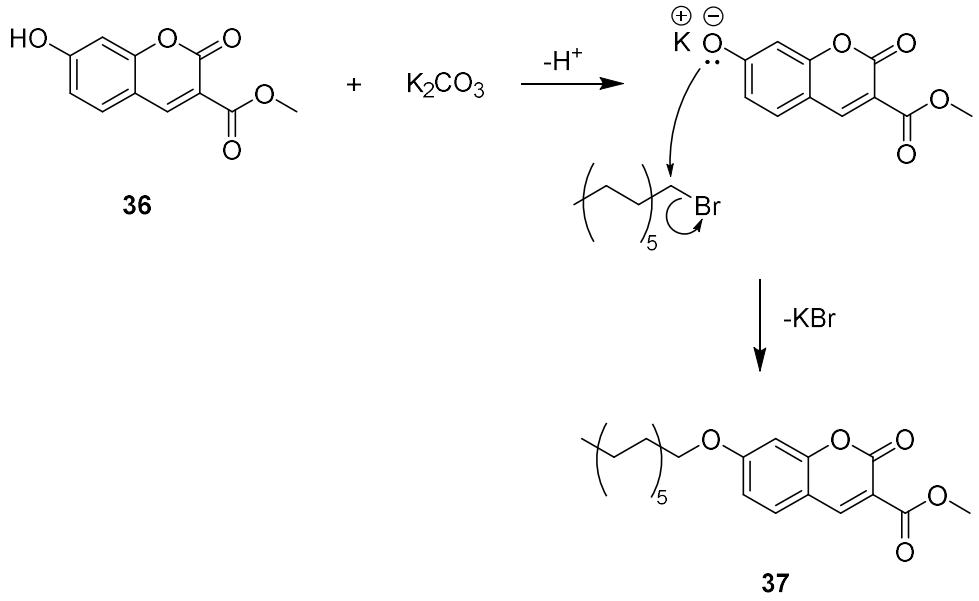

Scheme 10: Williamson ether synthesis

The next step is to deprotect the carboxylic acid ready for the final step. The hydrolysis of the ester was catalysed by a base and occurred via the mechanism shown in Scheme 11. Here the OH from the base (in this case KOH) attacks the carbonyl group with the electrons in the double bond residing on the oxygen. These electrons reform the carbonyl in the next step and kick out methanol, to give coumarin **38**.

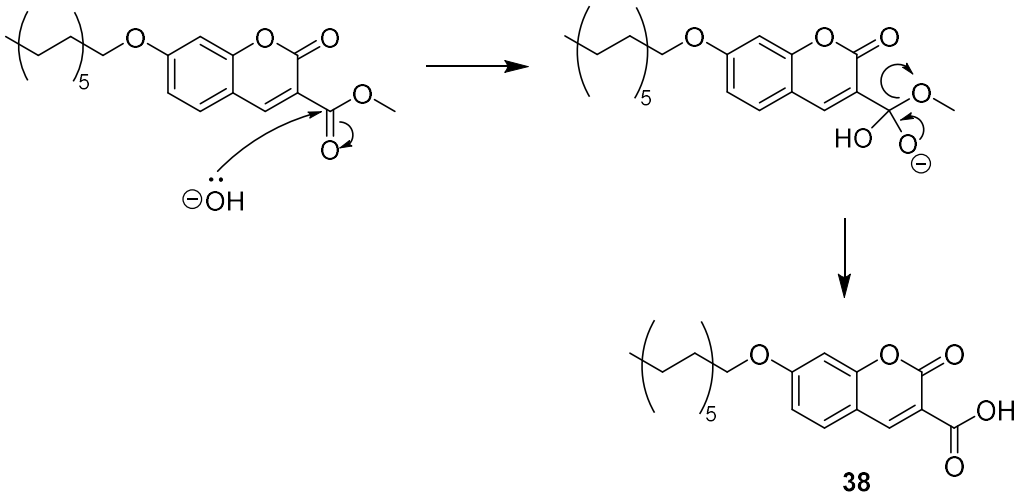

Scheme 11: Base catalysed hydrolysis of ester

The final step in this synthesis was to couple together amine **34** and coumarin **38**. This occurred via an amide coupling reaction utilising EDC-HCl, HOBt and DIPEA (Scheme 12). EDC-HCl is a carbodiimide, who's role in amide coupling reactions is to activate the carboxylic acid by converting the OH into a good leaving group.[17] To begin the lone pair of one of the nitrogens in EDC-HCl deprotonates the alcohol group of coumarin **38**. Oxygen is now negatively charged and can attack the carbon, and the electrons in the double bond move onto the positively charged nitrogen. Now HOBt can come in and attack the carbonyl group, resulting in the formation of a urea by-product. This increases the reactivity of the activated ester.[17] Amine **34** can now attack the carbonyl group using the lone pair of electrons on the nitrogen, and HOBt is now reformed. Finally, DIPEA deprotonates the positively charged amine to give the final product amphiphilic ligand **31**.

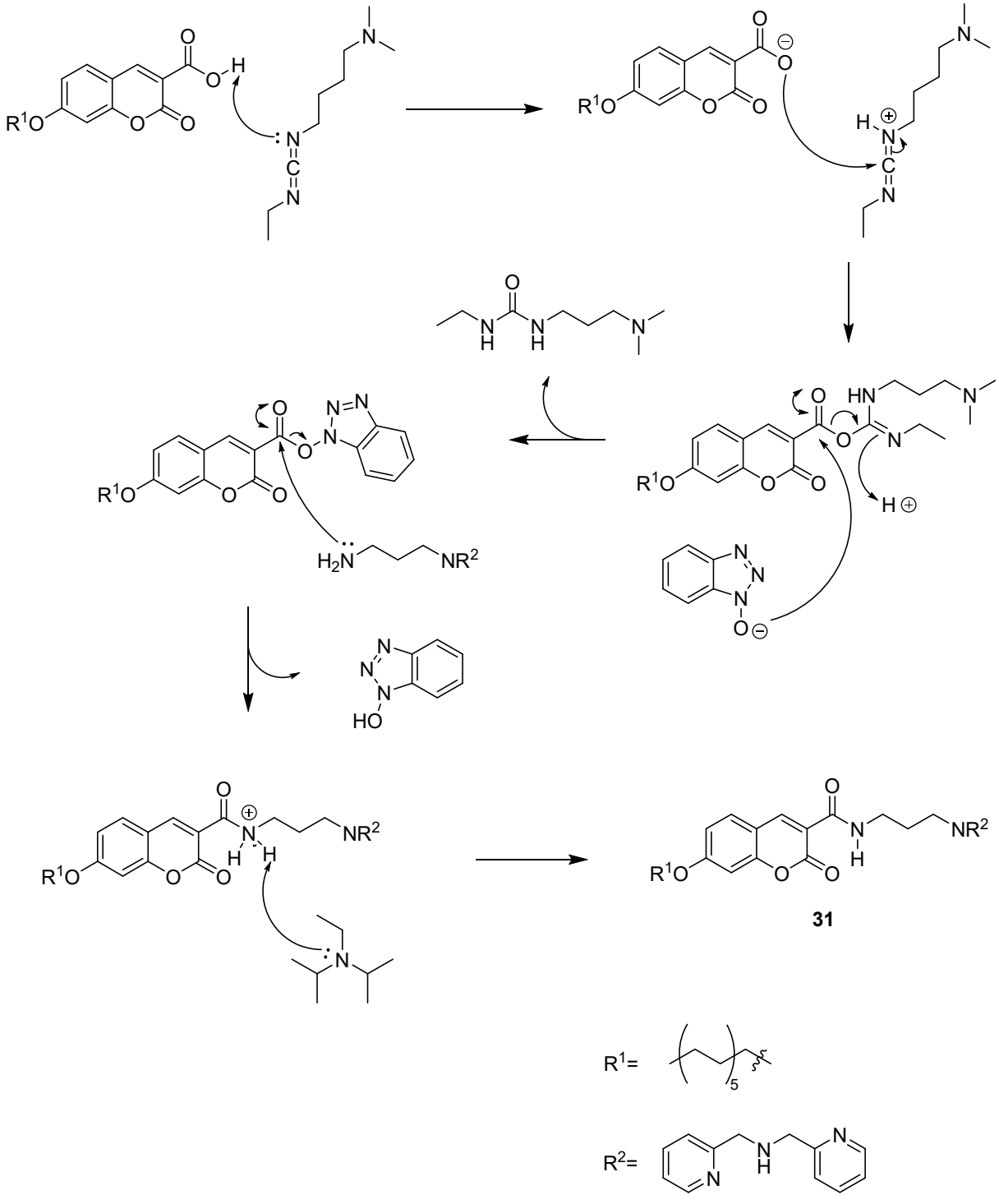

Scheme 12: Amide coupling using EDC-HCl, HOBt and DIEPA.

The control molecule **32** was synthesised following the same synthetic steps as for **31** (Scheme 13). With the only difference being 1-bromobutane was used for the alkylation of coumarin **36** as opposed to 1-bromododecane. This then results in two different coumarins being formed, **39** and **40**. Since only the length of the carbon chain was altered the reaction conditions for both the long and short chain coumarins were identical. Molecule **32** therefore will have the same dipicolylamine binding unit and coumarin moiety as **31,** with a C_4 chain as opposed to the C_{12} chain of **31**. The shorter chain will prevent this molecule from being able to self-assemble thus the sensing nature of these two compounds can be compared to determine whether a self-assembled system is favourable for phosphate binding/sensing.

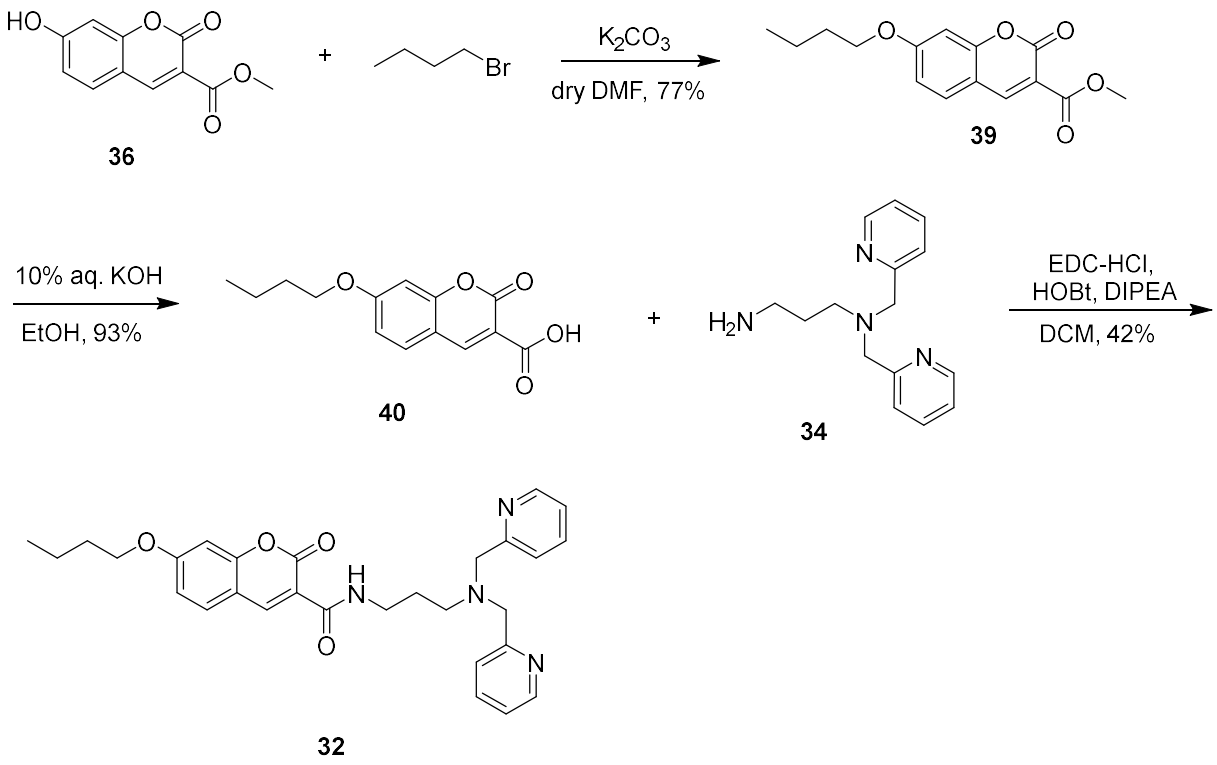

Scheme 13: Synthesis of Control Molecule **32**

2.3 NMR Assignment

All compounds synthesised in this project were characterised via NMR spectroscopy. The NMR assignment for amphiphilic ligand **31** is described below.

The ^{1}H NMR spectra (Figure 12) was the first spectra assigned for ligand **31**. The complexity of both ligand **31** and its ^{1}H NMR spectra initially made assigning peaks difficult. Therefore, we used previous NMR assignments for amine **34** and coumarin **38** to help with ligand **31** assignment.

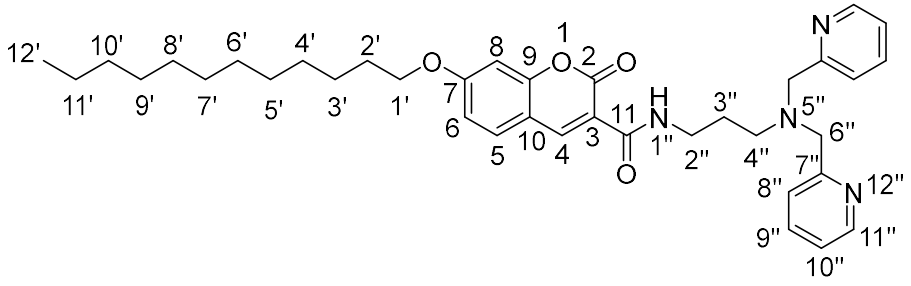

Amphiphilic ligand **31**

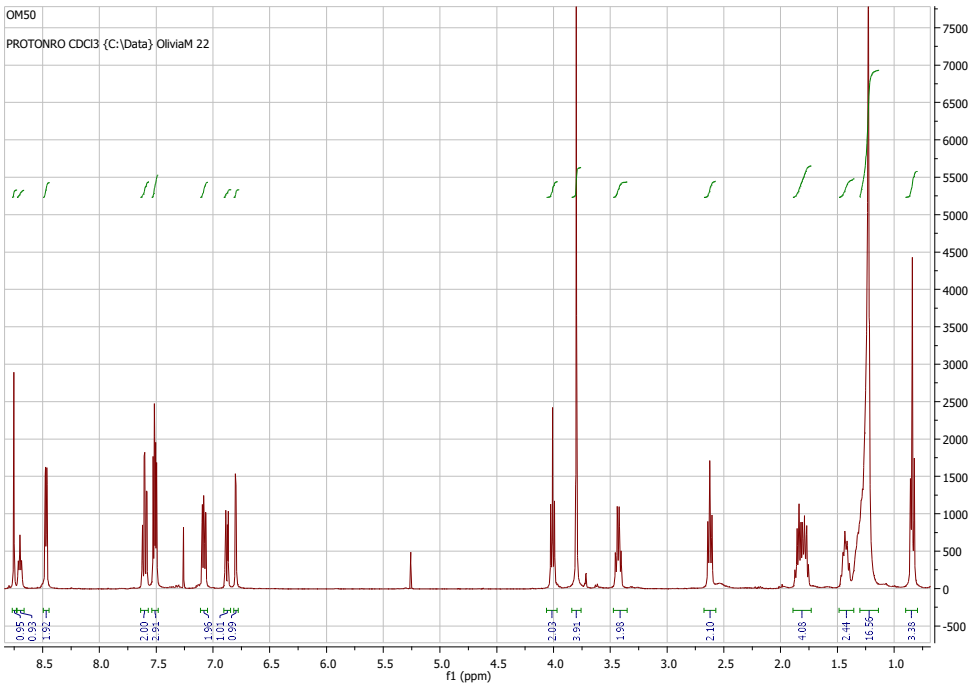

Figure 12: ^{1}H NMR of amphiphilic ligand **31**

The ^{1}H NMR spectra for amine **34** (shown in Figure 13) is much simpler consisting of four aromatic peaks and four aliphatic peaks. The peak at 3.79 integrated for 4 protons and appeared as a singlet so could easily be identified as 6. The remaining aliphatic peaks could be identified. 2 and 4 are both next to a nitrogen so should experience a similar chemical shift, while 3 is next to two CH_2 groups resulting in it being downshifted compared to 2 and 4. Thus the peak at 1.67-1.78 corresponds to 3 and the multiplet at 2.55-2.70 corresponds to 2 and 4. The aromatic region can be assigned using the chemical shift of nitrogen resulting in the most upfield peak being 11. From here we can assign the rest of the peaks using their splitting patterns and coupling constants. 11 is a doublet with a J_3 coupling constant of 5.0 Hz. The peak at 7.28 has a coupling constant one of which is 5.1 Hz. Protons which couple together have the same or similar coupling constants, so this peak corresponds to 10. The second coupling constant for this peak is 7.5. The peak at 7.80 has two coupling constants which match that of peak 10. Thus, this peak corresponds to proton 9. The remaining aromatic peak must correspond to 8

and we see this has a coupling constant of 0.78 which matches that of 9 confirming the assignment of this peak.

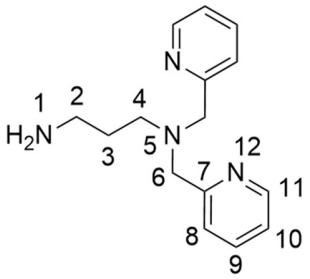

Amine **34**

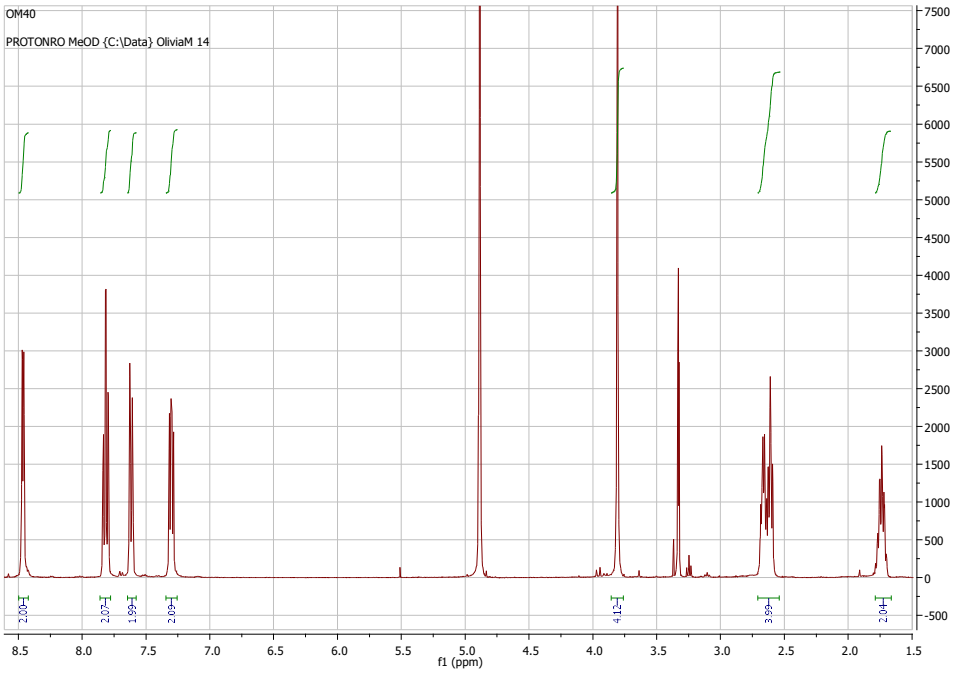

Figure 13: ^{1}H NMR of amine **34**

The next key NMR to assign was that of alkylated coumarin **38**, shown below in Figure 14.

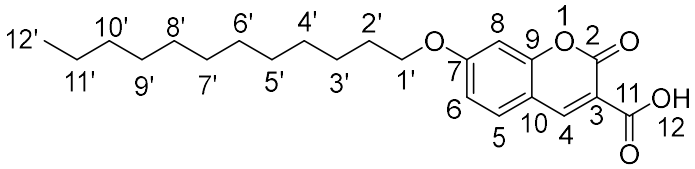

Coumarin **38**

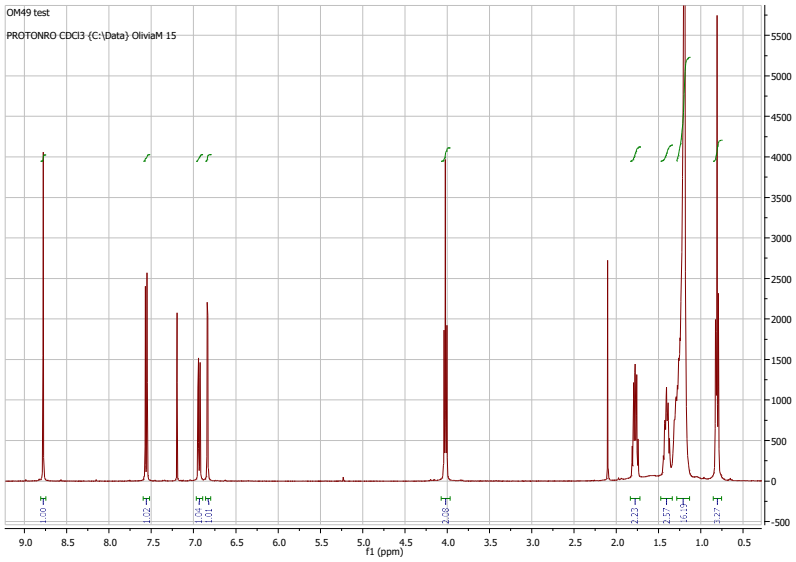

Figure 14: ^{1}H NMR for coumarin **38**

To begin the aromatic region of the spectra was assigned. This compound has four aromatic protons, two which we expect to be singlets and two doublets. These peaks were assigned based on the assignment for the starting material coumarin **35**. Literature for this stated that the singlet peak at 8.78 corresponds to the alkene proton, so proton 4 in this assignment.[18] The remaining three protons are all assigned as aromatic protons in the literature.[18] The COSY NMR data, shown in Figure 15, can be used to identify the remaining three peaks. The singlet yet to be assigned at 6.84 must belong to proton 8 as this is the only other aromatic proton we would expect to see a singlet for. The COSY NMR spectra shows that this proton is close to the proton at 6.93. Thus, this

can be assigned as proton 6. Proton 6 is close to both proton 8 and the proton at 7.56, so this can be assigned proton 5.

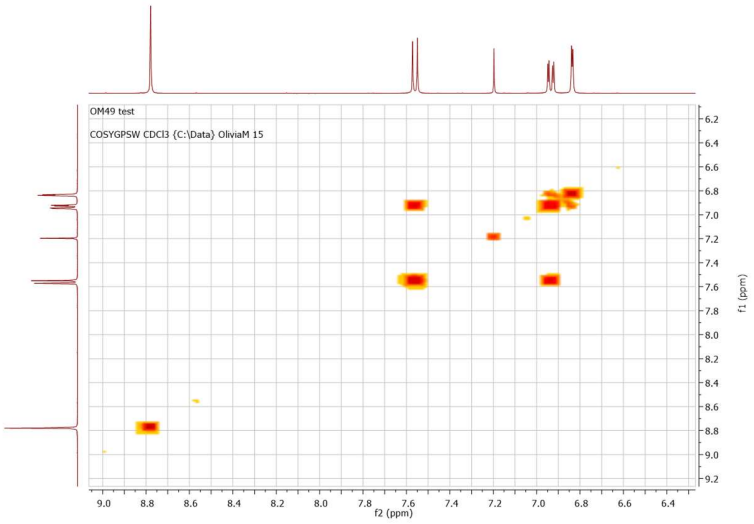

Figure 15: COSY NMR for coumarin **38**

The aliphatic region of the ^{1}H NMR spectrum could then be assigned, starting with the peak at 0.81. This is a triplet integrating for three protons so must correspond to the CH_3 group at the end of the long chain. The next peak integrates for 16 protons and can be assigned to most of the CH_2 groups present in the alkyl chain. We see that the three CH_2 groups closest to the oxygen experience a higher chemical shift, differentiating them from the rest of the alkyl chain. This allows the assignment for the three remaining peaks to be based on their relative positions to the oxygen atom. With proton 3' being assigned the peak at 1.35-1.47, proton 2' at 1.73-1.82 and proton 1' at 4.02.

The assignment of NMR spectra for both amine **34** and coumarin **38** could then be used to assign the spectra for amphiphile **31**. This was particularly useful for two of the multiplet peaks at 7.48-7.54 in the aromatic region and at 1.74-1.89 in the aliphatic region. Both of these peaks correspond to two sets of protons present at different parts of the molecule. The aromatic peak integrates for 3 protons and can be assigned to protons 5 and 8''. Thus, this peak is made up of a proton from the coumarin and a

proton from the amine. Looking at the previous NMR assignments of amine **34** and coumarin **38** it can be seen that both have a peak around the same region of the spectra and now those two peaks lie on top of one another. This is the same reason we see a multiplet in the aliphatic region integrating for four protons, as in previous spectra the two peaks occur at the same position. The HSQC for this compound also help to determine that these peaks corresponded to two different protons as they correspond to two different carbon peaks (Figure 16). This figure shows the aromatic proton at 7.48-7.54 corresponding to two different carbon atoms, while the rest of the peaks in this region just correspond to one carbon peak. The rest of the ^{1}H NMR spectra could be assigned as before and all of the expected peaks were observed.

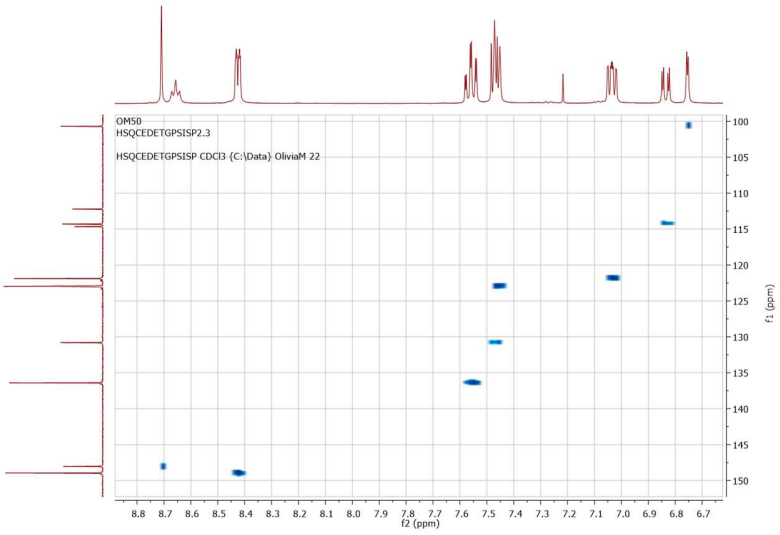

Figure 16: HSQC for the aromatic region of amphiphilic ligand **31**.

The ^{13}C NMR of amphiphile **31** is shown in Figure 17. This spectrum could be assigned using the HSQC and HMBC spectra of **31**.

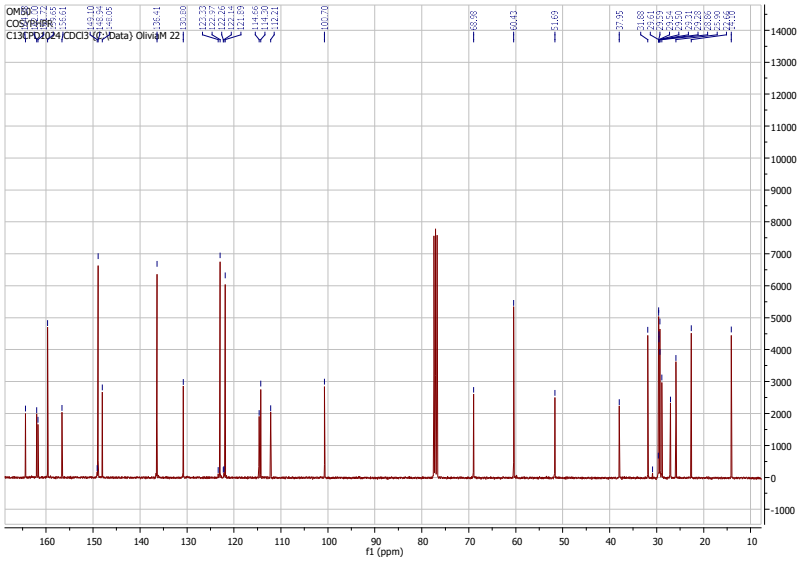

Figure 17: ^{13}C NMR spectrum of amphiphilic ligand **31**

Initially, the HSQC spectra was used to assign all the carbons which have a proton bonded directly to them. Figure 18 shows the aromatic portion of the HSQC spectrum. The proton peak at 8.75 corresponds to the carbon peak at 151.2. Since the proton peak was assigned as 4 then the carbon peak can also be assigned as 4. This process can be repeated with the rest of the peaks in the spectrum, assigning all the CH, CH_2 and CH_3 peaks.

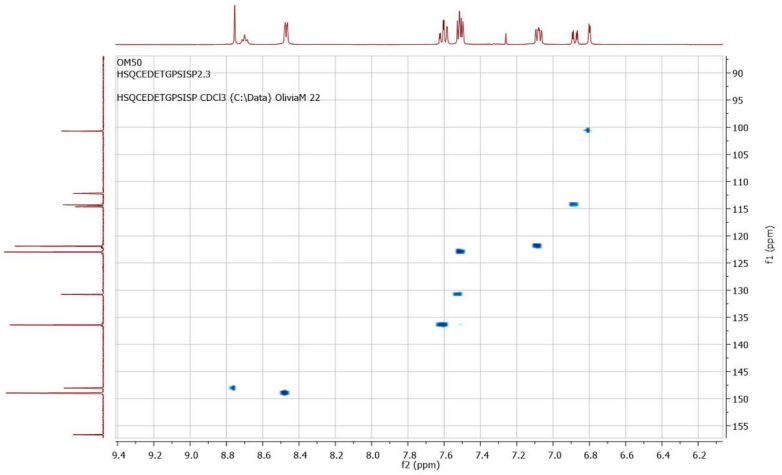

Figure 18: HSQC of amphiphilic ligand **31** showing the aromatic region.

The quaternary carbons can be assigned using the HMBC spectrum. This shows a correlation between the carbon peak and protons which are 3-4 bonds away. Figure 19 shows the aromatic portion of the HMBC spectrum. The carbon peak at 164.6 sees the proton peak at 8.75, the only proton peak it is correlated to in the spectrum. This proton peak has been assigned 4. Looking at the structure of amphiphile **31** the carbon which should correlate to only proton 4 is carbon 3. Thus, this peak can be assigned 3. This process can be repeated with the remaining peaks in the spectrum.

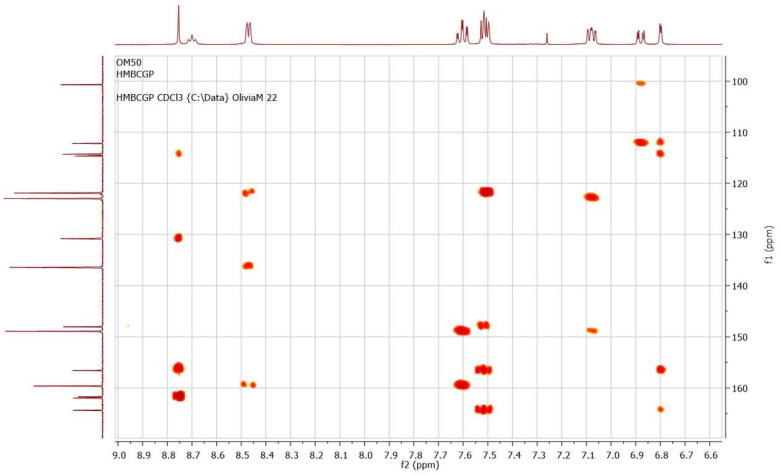

Figure 19: HMBC spectrum of amphiphilic ligand **31**, showing the aromatic region.

Control molecule **32** was assigned in a similar way to amphiphile **31**, beginning with the assignment of the starting materials and using other NMR techniques such as COSY, HSQC and HMBC to confirm the assignment.

2.4 UV Studies

To assess the ability of our designed sensors to detect phosphate oxoanions, we utilised UV-vis spectroscopy. The UV studies we employed were based off previous work by Jolliffe et al.[1] In their work they designed sensors which also utilise the picolyl amine units to sense/bind phosphates. They investigated the binding of their sensors with several different dyes prior to conducting IDAs. Jolliffe et al. found PV to be the most effective at binding their sensor, forming 1:1 complexes.[1] Therefore we decided to assess the binding of both our amphiphilic ligands **29** and **31** with PV to determine if this would be a suitable dye for us to use for our IDAs.

Initially we analysed the dye-sensor binding of **29** with PV, then with the addition of the phosphate ATP. We began by briefly looking at the spectral changes resulting from the

addition of ligand **29**, at varying concentrations, to PV. Figure 20 shows clear spectra changes with the addition of ligand **29** to the system. A small increase in absorbance is seen for the peak at 600 nm, along with a new peak forming at 700 nm. Jolliffe et al. reported an increase in the peak along with a bathochromic shift, however we see a very minimal shift in wavelength with increasing concentrations.[1] From here we decided to see what addition of a phosphate did to the spectrum, to see if we get a reversible change like in Jolliffe's system. For this we used the same concentration of PV (10 μM) as for the previous experiments along with 12 μM of ligand, as this was the lowest concentration which gave the greatest spectral change. Figure 21 shows the addition of ATP at various different concentrations. Here we were looking for a decrease in the peak at 695 nm. We found that this was not very efficient, even with higher concentrations of ATP. Therefore, we decided to investigate amphiphilic ligand **31** to see if this gave better results.

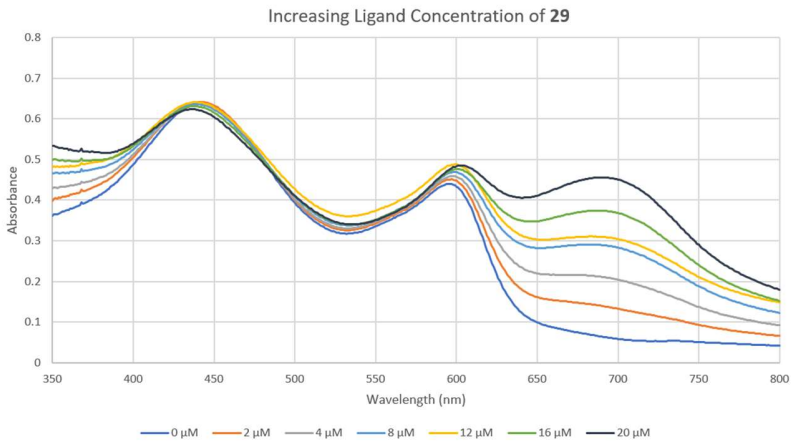

Figure 20: Changes in absorbance of PV solution with increasing ligand concentration. Conditions: [HEPES buffer] = 50 mM, pH 7.4, [NaCl] = 145 mM, [PV] = 10 μM, 1:1 ratio [ligand]: [zinc] = 0, 2, 4, 8, 12, 16, and 20 μM.

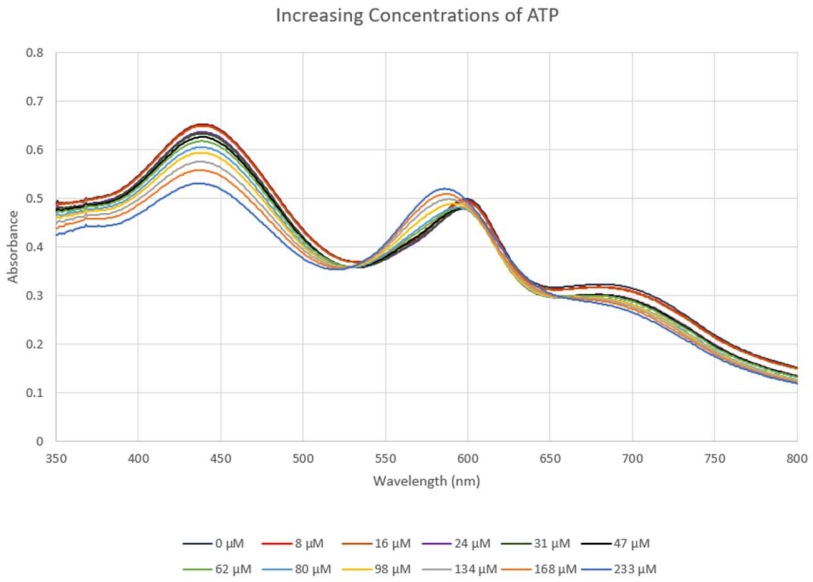

Figure 21: Changes in absorbance with increasing ATP concentration. Conditions: [HEPES buffer] = 50 mM, pH 7.4, [NaCl] = 145 mM, [PV] = 10 µM, 1:1 ratio [ligand]: [zinc] = 12 µM, [ATP] = 0, 8, 16, 24, 31, 47, 62, 80, 98, 134, 168, and 233 µM.

Prior to assessing the dye-sensor binding we took the UV-vis absorption spectra for both compounds **31** and **32** to see where our compounds absorb in the UV-vis spectrum (Figure 22). Coumarins typically have an absorbance peak between 270-320 nm, though this can shift depending on their ring substitution.[19] Both of our compounds have an absorbance maximum at ~350 nm, which can be attributed to absorption by the coumarin moiety. We also decided to investigate whether the addition of zinc resulted in any significant changes to our spectra. No change in absorbance or shift in the peaks was observed with the addition to zinc. The main difference we observed from the spectra of our two compounds is the shape of the coumarin peak. For ligand **31** we have a broad coumarin peak with a low absorbance compared with that of our control molecule **32**, which has a sharp peak and a higher absorbance. This could be due to **31** self-assembling in solution. The self-assembled structure will result in the partial solubilisation of the coumarin. This results in the coumarin experiencing a range of different polarities. Coumarins are known to experience solvatochromic effects, whereby

the UV absorption can change depending on the polarity of the solvent.[20, 21] Thus, resulting in the broadening of the signal for amphiphile **31**.

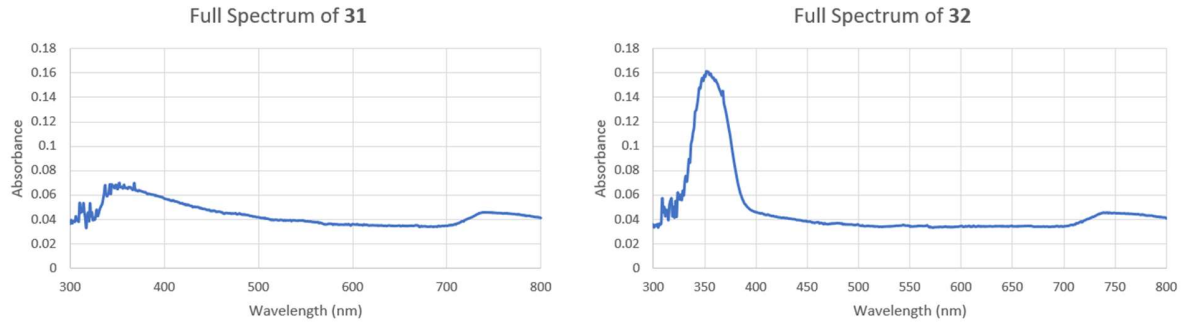

Figure 22: UV-vis spectrum of **31** and **32.** Conditions: [HEPES buffer] = 50 mM, pH 7.4, [NaCl] = 145 mM, [ligand] = 20 μM.

To assess the binding between our sensor and PV, a UV-vis titration was performed. PV is a catechol-type indicator which requires two zinc ions to bind the catechol group.[1] This should result in a colour change. Amphiphile **31** consists of a long carbon chain allowing this molecule to self-assemble. The dipicolylamine groups are able to bind zinc ions and when the sensor self assembles these groups and hence the zinc ions are brought close together, and can bind the catechol group of the dye. Molecule **32** cannot self-assemble due to the short chain. Therefore, we expect **31** to have stronger binding to PV than **32**, due to self-assembly. Figure 23 shows the absorbance spectra for the titration of PV with each ligand. A bathochromic shift is seen in the spectrum for both ligands with the absorbance peak at 598 nm shifting to 680 nm. This is a larger shift than the one reported by Jolliffe et al. from 600 nm to 640 nm.[1] A colour change is observed at 60 μM of both sensors, from green to blue (Figure 24). **31** has a greater absorbance at 680 nm than **32**. This indicates that self-assembly is playing a role in the sensors ability to bind PV. Jolliffe et al. reported an increase in the absorbance at 640 nm as a result of PV being bound by the zinc ions in their sensor.[1] Therefore we can also conclude that the higher absorbance for **31** is due to greater binding of PV than for

32. The self-assembly of **31** results in zinc ions being positioned close to one another ready for two of these to bind one PV molecule. For **32** the molecules are not aligned in solution making it harder for two sensors to come together and bind one PV molecule. When PV is bound by the sensor a change in absorbance is seen in both our system and in that reported by Jolliffe and co-workers. We noticed that a large amount of our ligand needs to be added to see significant spectral changes along with the colour change from green to blue. Jolliffe's system had 1:1 binding of sensor to PV compared to our 5:1 sensor to PV binding. However, Jolliffe's sensor consisted of two zinc dipicolylamine units per molecule while ours only consists of one. To compare the two systems, we need to look at the concentration of zinc dipicolylamine units as opposed to the concentration of ligands. Jolliffe et al. has 2:1 binding of zinc dipicolylamine units to PV, whilst our system has 5:1 binding of zinc dipicolylamine units to PV. PV is therefore not a suitable dye to utilise in our IDAs due to its poor binding with our sensor. Therefore, we decided to investigate the binding between our sensor and another dye, bromopyrogallol red (BPR).

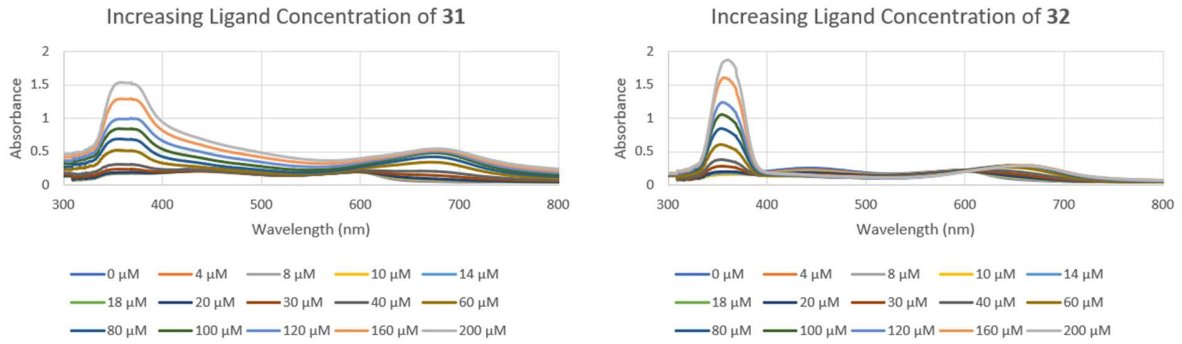

Figure 23: Changes in absorbance of PV solution with increasing ligand concentration. Conditions: [HEPES buffer] = 50 mM, pH 7.4, [NaCl] = 145 mM, [PV] = 20 µM, 1:1 ratio [ligand]: [zinc] = 0, 4, 8, 10, 14, 18, 20, 30, 40, 60, 80, 100, 120, 160, and 200 µM.

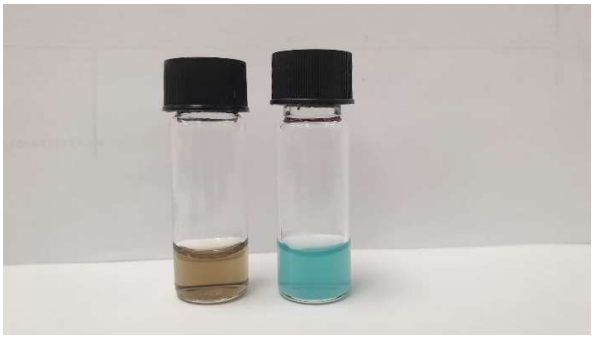

Figure 24: UV-visible titration of PV (20 μM) with amphiphile **31**. Left: initial solution with 0 μM sensor and 0 μM zinc. Right: final solution with 200 μM sensor and 200 μM zinc.

BPR is another catechol-type dye which requires two zinc ions to bind one catechol group. Amphiphile **31** has the ability to self-assemble therefore we expect this to have a greater absorbance than **32** to indicate greater binding. We found BPR to have significantly better binding with a clear spectral change (Figure 25) and colour change (Figure 26) occurring at 30 μM. The peak at 558 nm decreased until a concentration of 30 μM ligand (**31**) where we see a bathochromic shift to 600 nm. The absorbance then begins to increase. A continual increase in the peak at 355 nm is seen resulting from increasing the concentration of coumarin present. A clear difference between the absorbance spectra of **31** and **32** is observed. Ligand **31** has a greater absorbance indicating that self-assembly is favourable for binding BPR. The self-assembly of these sensor molecules results in the dipicolylamine binding groups and thus the zinc ions they bind being positioned next to one another. This is advantageous for binding BPR as these molecules are bound by their catechol groups which require two zinc ions to come together for this. With these molecules in their self-assembled state the zinc ions are already positioned correctly to bind BPR resulting in an absorbance change. This system gives us 3:1 binding of binding of zinc dipicolylamine units to BPR, much stronger than with PV. Therefore, BPR can be employed in our IDAs to assess the ability of our sensor to detect phosphates.

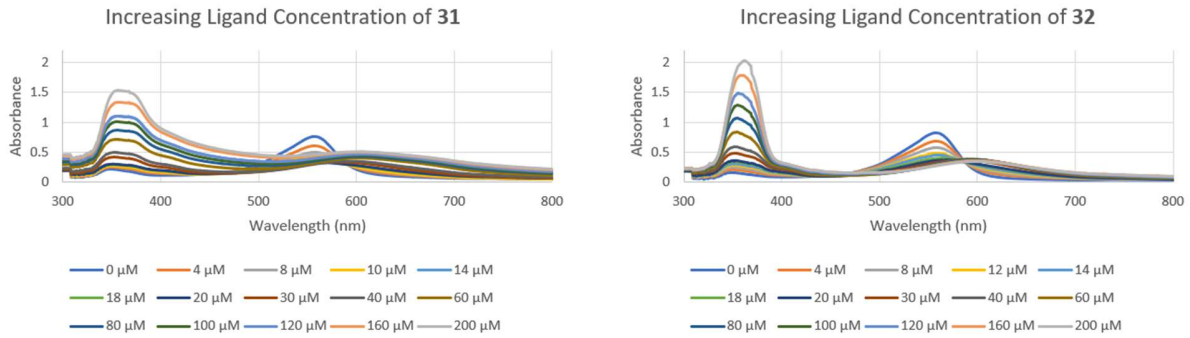

Figure 25: Changes in absorbance of BPR solution with increasing ligand concentration. Conditions: [HEPES buffer] = 50 mM, pH 7.4, [NaCl] = 145 mM, [PV] = 20 µM, 1:1 ratio [ligand]: [zinc] = 0, 4, 8, 10, 14, 18, 20, 30, 40, 60, 80, 100, 120, 160, and 200 µM.

Figure 26: Colour change with 20 µM BPR and increasing concentrations of ligand **31**. Left to right: 0 µM, 30 µM, 50 µM, 100 µM ligand.

Initially we looked at how our sensor could detect PPi. This was done utilising IDAs, where the addition of PPi should result in BPR being displaced, along with a change in the absorbance spectrum. 50 µM ligand and 20 µM BPR were the conditions used for these IDAs, with the absorbance results shown in Figure 27. The colour is initially blue and with the addition of PPi we see this colour change to purple. The absorbance spectrum for **31** shows that with the initial addition of PPi, a large amount of BPR is displaced, seen by the large increase in the absorbance spectrum at 558 nm. The

absorbance of this peak continues to increase with further additions of PPi. **32** however does not experience this dramatic increase in absorbance, instead we see small changes in the spectrum with each addition of PPi. Again, this shows that self-assembly helps the system to detect PPi as the binding groups are positioned next two one another. Phosphates require two zinc dipicolylamine units to bind one phosphate molecule.

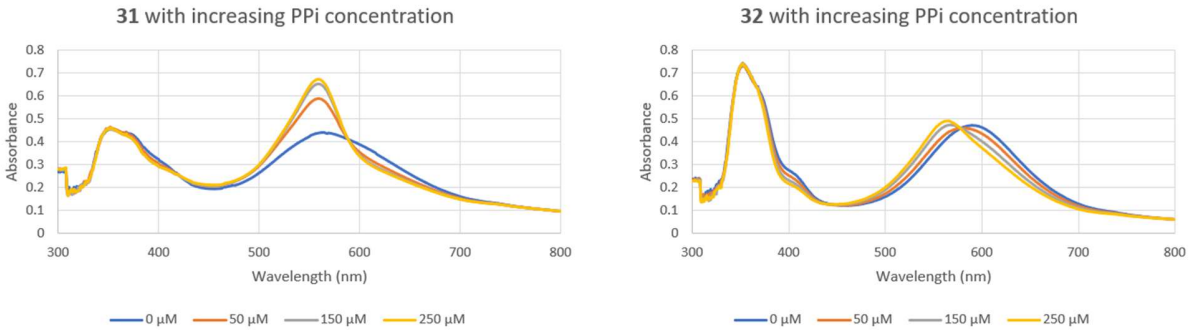

Figure 27: Change in absorbance with increasing PPi concentrations. Conditions: [HEPES buffer] = 50 mM, pH 7.4, [NaCl] = 145 mM, [BPR] = 20 µM, 1:1 ratio [ligand]: [zinc] = 50 µM, [PPi] = 0, 50, 150 and 250 µM.

Selectivity studies could then be done using the same conditions (50 µM ligand and 20 µM BPR) and a number of different phosphates (PPi, ATP, $H_2PO_4^-$, citrate, dimethyl phosphate (DMP), and PO_4^{3-}). This involved adding five equivalents of the selected phosphate to the system and observe any colour changes (Figure 28). For **31** we see a clear colour change for PPi, ATP and citrate, while $H_2PO_4^-$, DMP, and PO_4^{3-} have no change. These results are reflected in the spectra of each addition (Figure 29). $H_2PO_4^-$, DMP, and PO_4^{3-} show no change in the absorbance spectra as increasing concentration of each phosphate is added. PPi and ATP have similar spectra with a slight shift and increase in absorbance of the peak at 558 nm. However, this change in absorbance is not as dramatic for ATP compared with PPi, resulting is less of a colour change when 5 equivalents have been added. Citrate also experiences a colour and spectral change with five equivalents added. No spectral changes are seen with the addition of just one equivalent of citrate. This indicates that citrate is only able to displace BPR at higher

concentrations making our sensor more selective for PPi and ATP at lower concentrations. The colour change when only one equivalent of phosphate is added shows only PPi as slightly purple, the result of the phosphates remains blue (Figure 30). Therefore, our sensor has good binding with PPi.

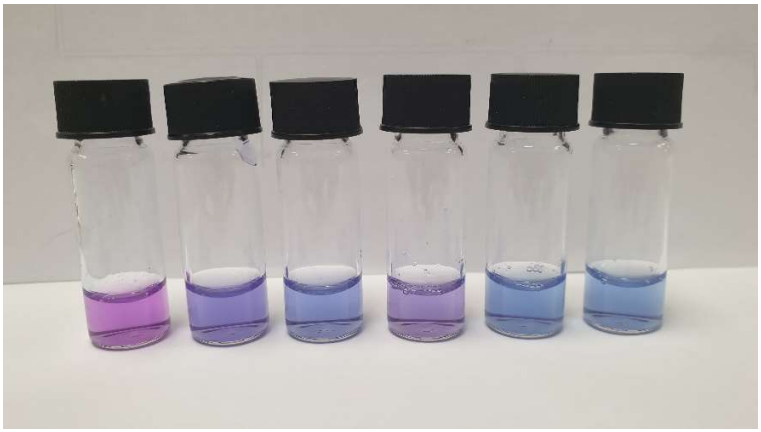

Figure 28: Sensor **31** selectivity studies – 5 equivalents of phosphate. Left to right: PPi, ATP, $H_2PO_4^-$, citrate, DMP, and PO_4^{3-}

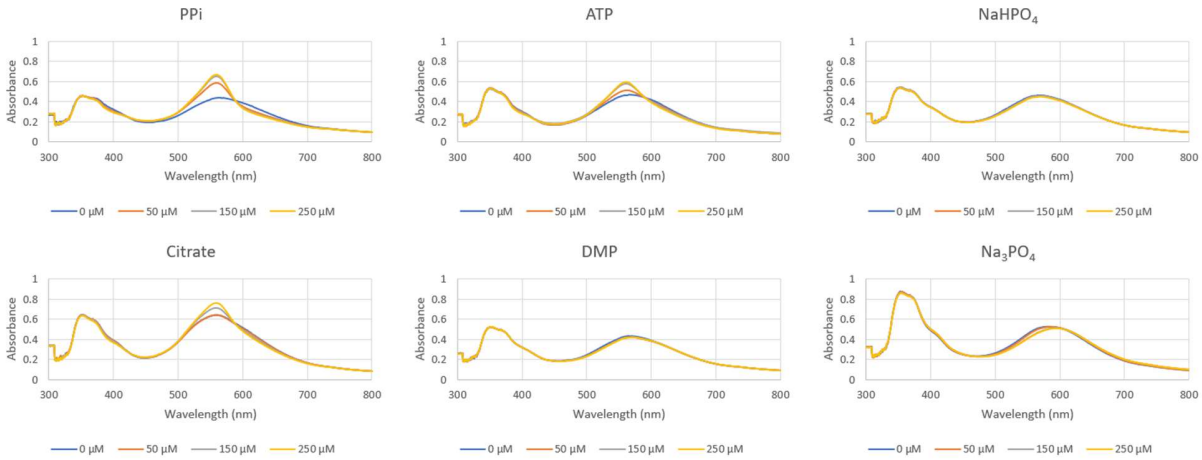

Figure 29: Absorbance spectra for the addition of different phosphates to ligand **31**. Conditions: [HEPES buffer] = 50 mM, pH 7.4, [NaCl] = 145 mM, [BPR] = 20 µM, 1:1 ratio [ligand]: [zinc] = 50 µM, [phosphate] = 0, 50, 150 and 250 µM.

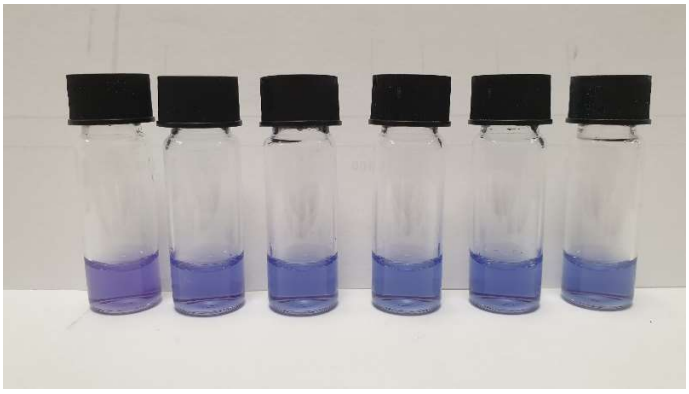

Figure 30: Sensor **31** selectivity studies – 1 equivalent of phosphate. Left to right: PPi, ATP, $H_2PO_4^-$, citrate, DMP, and PO_4^{3-}

Comparing our selectivity results for **31** with our control molecule **32** we see that the self-assembled system gives greater binding of phosphates. The colour change for **32** when five equivalents of phosphate is added shows a slight colour change for PPi while the rest of the phosphates give no change (Figure 31). This this is reflected by the spectra data (Figure 32), which shows slight changes in the absorbance with the addition of PPi and ATP.

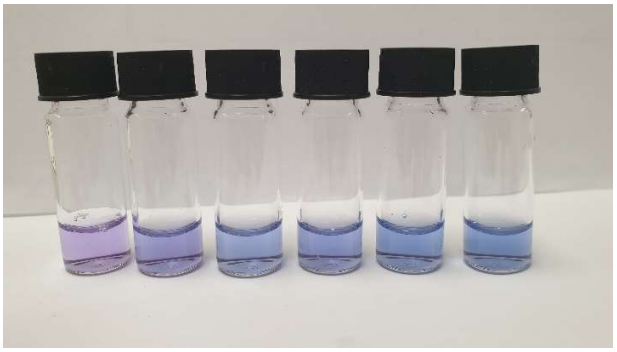

Figure 31: Sensor **32** selectivity studies – 5 equivalents of phosphate. Left to right: PPi, ATP, $H_2PO_4^-$, citrate, DMP, and PO_4^{3-}

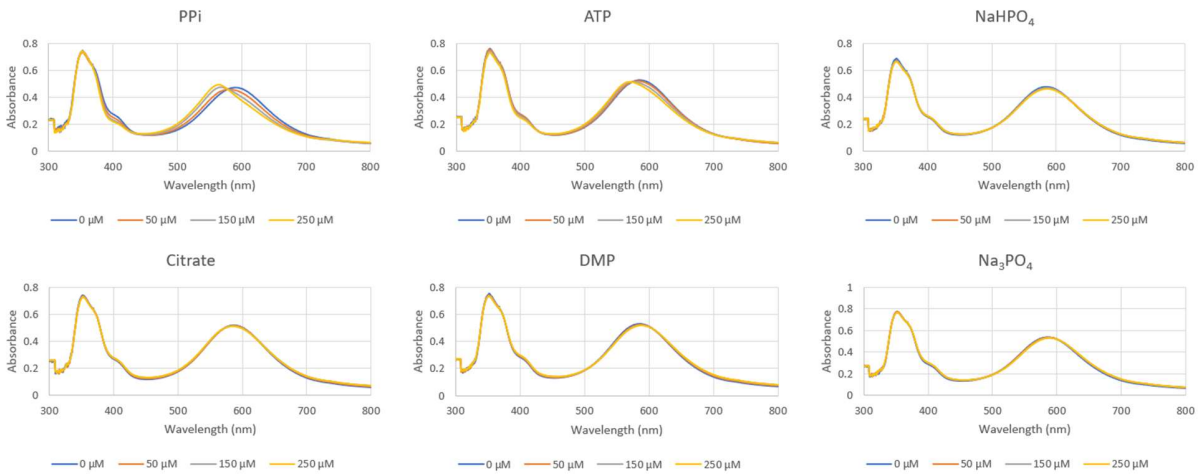

Figure 32: Absorbance spectra for the addition of different phosphates to **32.** Conditions: [HEPES buffer] = 50 mM, pH 7.4, [NaCl] = 145 mM, [BPR] = 20 µM, 1:1 ratio [ligand]: [zinc] = 50 µM, [phosphate] = 0, 50, 150 and 250 µM.

2.5 Conclusion and Future Work (Fluorescent Studies)

In this research, we successfully synthesised a sensor that utilises self-assembly to detect phosphate oxoanions. IDAs showed the ability for sensor **31** to selectively detect PPi and ATP from a library of different phosphates. Self-assembly proved to be crucial, which was demonstrated by a direct comparison between sensor **31** and our control molecule **32**. This found that the self-assembled sensor **31** had stronger binding to the phosphate oxoanion PPi and was able to respond to lower concentrations of this anion.

Currently we have assessed the sensor's functionality using UV-visible IDAs. The ability of this molecule to act as a sensor can also be investigated using fluorescence spectroscopy, measuring the changes in emission from the fluorescent coumarin moiety embedded in the sensor. We would expect to see a change in emission when the sensor binds phosphates.

We have shown that this self-assembled sensor system is capable of detecting phosphates. Next, we want to investigate different amphiphilic molecules in combination with this one to see if we get a more selective sensor. This idea exploits the modularity of self-assembled systems, allowing us to mix different functional groups to optimise the detection of the analyte.

Chapter 3: Experimental

3.1 Synthesis of Amphiphilic Ligand 29

3.1.1 Synthesis of hexadecyl bis(2-pyridylmethyl)amine (29)

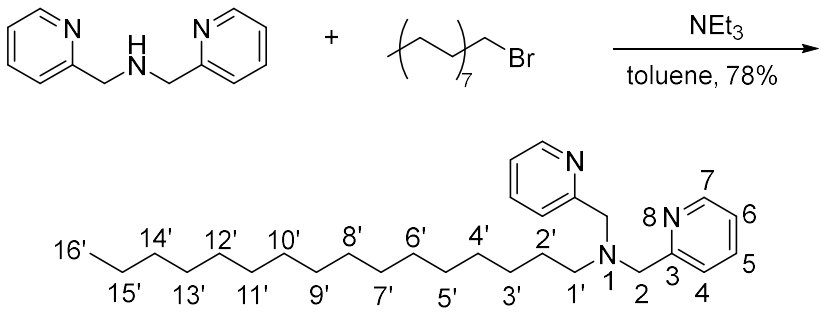

Di-(2-picolyl)amine (0.156 g, 0.786 mmol), 1-bromohexadecane (0.200 g, 0.655 mmol), and triethylamine (0.272 mL, 1.97 mmol) were dissolved in toluene (7 mL). The reaction was refluxed at 120 °C for three days. The toluene was removed *in vacuo* and the product was extracted into chloroform and washed with water. Flash chromatography was used to purify the product. Chloroform was initially used as the eluent until the first band was eluted, then a methanol/chloroform eluent system was used with varying polarity from 2% to 4% methanol. This gave **29** as a brown oil (0.209 g, 0.510 mmol, 78%).

δ_H (400 MHz, $CDCl_3$) 0.87 (3H, t, *J* = 6.6 Hz, 16'-H), 1.15-1.32 (26H, m, 3'-H to 15'-H), 1.53 (2H, quintet, *J* = 6.84 Hz, 2'-H), 2.53 (2H, t, *J* = 7.3 Hz, 1'-H), 3.81 (4H, s, 2-H), 7.13 (2H, t, *J* = 5.8 Hz, 6-H), 7.54 Hz (2H, d, *J* = 7.7 Hz, 4-H), 7.65 (2H, t, *J* = 7.6 Hz, 5-H), 8.51 (2H, d, *J* = 4.7 Hz, 7-H).

δ_C (100 MHz, $CDCl_3$) 14.2 (CH_3, C16'), 22.8 (alkyl CH_2), 27.5 (CH_2, C1'), 29.5 (alkyl CH_2), 29.6 (alkyl CH_2), 29.8 (alkyl CH_2), 29.8 (alkyl CH_2), 29.8 (alkyl CH_2), 32.0 (alkyl CH_2), 54.7 (CH_2, C1'), 60.6 (CH_2, C2), 121.9 (CH, C6), 123.0 (CH, C4), 136.4 (CH, C5), 149.1 (CH, C7), 160.2 (C-quat, C3).

IR vmax(film)/cm-1: 2918, 2849, 2810, 1589, 1567, 1469, 1433, 1092, 779, 756.

HRMS found (ESI): $[M+Na]^+$, 446.3496, $C_{28}H_{45}N_3Na$ requires 446.3506.

The ^{1}H NMR data matches that previously reported in the literature.[22, 23]

3.2 Synthesis of Control Molecule 30

3.2.1 Synthesis of butyl bis(2-pyridylmethyl)amine (30)

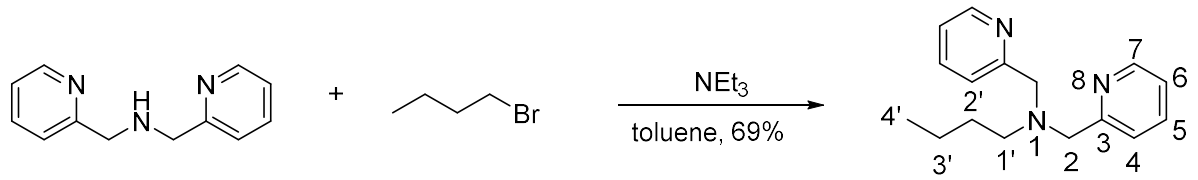

Di-(2-picolyl)amine (0.349 g, 1.75 mmol), 1-bromobutane (0.200 g, 1.46 mmol) and triethylamine (0.606 mL, 4.38 mmol) were dissolved in toluene (5 mL). This was refluxed at 120°C for 48 hours. The toluene was removed *in vacuo*, and the product was extracted in chloroform. This was washed with water, and the organic layer was concentrated *in vacuo*. Flash chromatography was used to purify the product. Chloroform was initially used as the eluent until the first band was separated, then methanol: chloroform eluent system was used with varying polarity from 2% methanol to 4%. This gave **30** as a brown oil (0.258 g, 1.01 mmol, 69%).

δ_H (400 MHz, $CDCl_3$) 0.83 (3H, t, *J* = 7.3 Hz, 4'-H), 1.22-1.34 (2H, m, 3'-H), 1.47-1.57 (2H, m, 2'-H), 2.53 (2H, t, *J* = 7.3 Hz, 1'-H), 3.8 (4H, s, 2-H), 7.12 (2H, t, *J* = 6.2 Hz, 6-H), 7.54 (2H, d, *J* = 7.9 Hz, 4-H), 7.64 (2H, t, *J* = 7.6 Hz, 5-H), 8.51 (2H, d, *J* = 4.8 Hz, 7-H).

δ_C (100 MHz, $CDCl_3$) 13.9 (CH_3, C4'), 20.6 (CH_2, C3'), 29.5 (CH_2, C2'), 54.3 (CH_2, C1'), 60.7 (CH_2, C2), 121.9 (CH, C6), 122.9 (CH, C4), 136.4 (CH, C5), 149.1 (CH, C7), 160 (C-quat, C3).

The NMR data is in line with that previously reported in the literature.[24]

3.3 Synthesis of Amphiphilic Ligand 31

3.3.1 Synthesis of *N*-(3-bis(2-pyridylmethyl)aminopropyl)phthalimide (33)

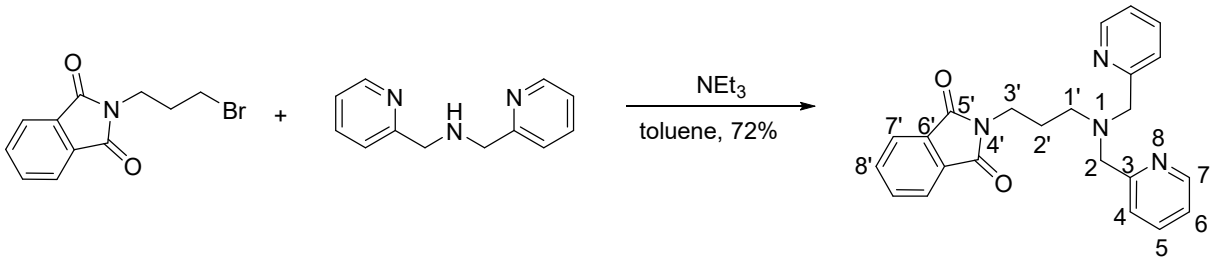

N-(3-Bromopropyl) phthalimide (0.700 g, 2.61 mmol), di-(2-picolyl)amine (0.624 g, 3.13 mmol), and triethylamine (1.08 mL, 7.83 mmol) were dissolved in toluene (7 mL). The reaction was refluxed at 120 °C for four days. The toluene was removed *in vacuo*. Product was extracted in chloroform and washed with water. Flash chromatography on alumina was used to purify the product. A gradient of solvent systems was used beginning with hexane, then 25% DCM in hexane, 50% DCM in hexane to elute first yellow band, then 75% DCM in hexane, 100% DCM and 0.5% MeOH in DCM to yield **33** (0.728 g, 1.89 mmol, 72%) as a brown viscous oil.

δ_H (400 MHz, $CDCl_3$) 1.87-1.97 (2H, m, 2'-H), 2.63 (2H, t, *J* = 7.0 Hz, 1'-H or 3'-H), 3.69 (2H, t, *J* = 7.5 Hz, 1'-H or 3'-H), 3.82 (4H, s, 2-H), 7.10 (2H, ddd, *J* = 7.4, 4.9, 1.3 Hz, 6-H), 7.53 (2H, d, *J* = 7.8 Hz, 4-H), 7.62 (2H, td, *J* = 7.7, 1.8 Hz, 5-H), 7.67-7.72 (2H, m, 7'-H or 8'-H), 7.78-7.84 (2H, m, 7'-H or 8'-H), 8.46 (2H, d, *J* = 4.9, 7-H).

δ_C (100 MHz, $CDCl_3$) 26.14 (CH_2, C2'), 36.3 (CH_2, C1' or C3'), 51.3 (CH_2, C1' or C3'), 60.3 (CH_2, C2), 121.8 (CH, C6), 123.0 (CH, C7' or 8' and C4), 132.2 (C-quat, C7'), 133.8 (CH, C7' or C8'), 136.4 (CH, C5), 148.8 (CH, C7), 159.4 (C-quat, C3), 168.4 (C-quat, C5').

The NMR data is comparable to that of the literature.[25]

3.3.2 Synthesis of *N,N*-dipicolylpropylamine (34)

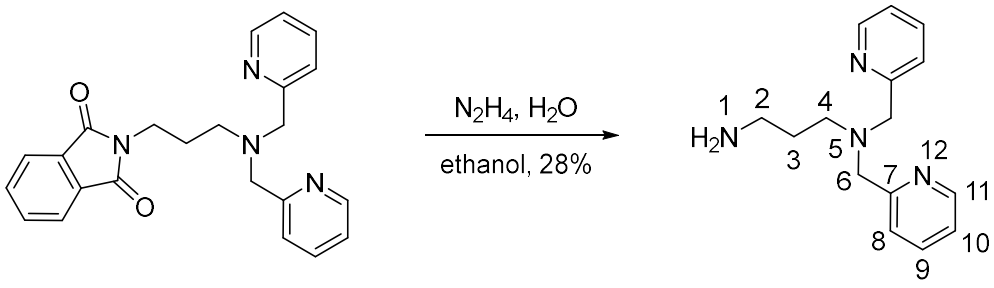

To a solution of *N*-(3-bis(2-pyridylmethyl)aminopropyl)phthalimide (700 mg, 1.81 mmol) in ethanol (10 mL) was added hydrazine monohydrate (0.630 mL, 12.7 mmol) and the reaction was refluxed at 90 °C overnight. Ethanol was removed *in vacuo*, the remaining solid was dissolved in chloroform and water was used to extract the product into the aqueous layer. The water was then removed *in vacuo* and the residue was purified using gradient elution flash chromatography on alumina. 5% MeOH in DCM was used to remove the first band, and the polarity of the solvent system was increased to 10% MeOH in DCM until the product started eluting. Finally, the polarity was increased to 15% MeOH in DCM increase the elution rate. This gave **34** as a yellow oil (0.127 g, 0.495 mmol, 28%).

δ_H (400 MHz, CD_3OD) 1.67-1.78 (2H, m, 3-H), 2.55-2.70 (4H, m, 2-H and 4-H), 3.79 (4H, s, 6-H), 7.28 (2H, dd, *J* = 5.1, 7.5 Hz, 10-H), 7.60 (2H, d, *J* = 7.8 Hz, 8-H), 7.80 (2H, ddd, *J* = 7.8, 5.9, 1.7 Hz, 9-H), 8.44 (2H, d, *J* = 5.0 Hz, 11-H).

δ_C (100 MHz, CD_3OD) 29.4 (CH_2, C3), 39.4 (CH_2, C2 or CH_2, C4), 52.0 (CH_2, C2 or CH_2, C4), 59.7 (CH_2, C6), 122.4 (CH, C10), 123.5 (CH, C8), 137.3 (CH, C9), 148.1 (CH, C11), 159.3 (C-quat, C7).

Looking at the literature NMR data reported in deuterated chloroform our NMR data was comparable.[25]

3.3.3 Synthesis of 7-hydroxy-2-oxo-2H-1-benzopyran-3-carboxylic acid (35)

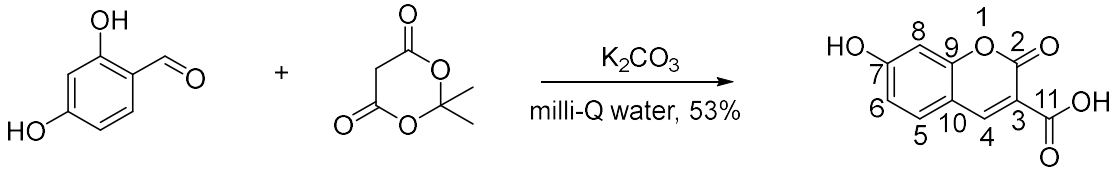

4-Hydroxysalicyl aldehyde (2.00 g, 14.5 mmol), Meldrum's acid (1.99 g, 14.5 mmol), potassium carbonate (0.400 g, 2.9 mmol) and milli- Q water (70 mL) were stirred at room temperature for 20 hours. Chilled 2 M HCl (10 mL) was used to acidify the solution, precipitating out a solid. The solid was then filtered and washed with water. Compound was purified via recrystallisation with ethyl acetate. This gave **35** as a yellow solid (1.59 g, 7.60 mmol, 53%).

δ_H (400 MHz, $(CD_3)_2SO$) 6.74 (1H, d, *J* = 2.1 Hz, 8-H), 6.84 (1H, dd, *J* = 8.7, 2.2 Hz, 6-H), 7.74 (1H, d, *J* = 8.7 Hz, 5-H), 8.68 (1H, s, 4-H).

δ_C (100 MHz, $(CD_3)_2SO$) 102.3 (CH, C8), 111.1 (C-quat, C7), 112.9 (C-quat, C9), 114.5 (CH, C6), 132.9 (CH, C5), 149.8 (CH, C4), 157.5 (C-quat, C10), 158.1 (C-quat, C3), 164.4 (C-quat, C2 or C11), 164.7 (C-quat, C2 or C11).

The NMR data matches that previously reported in the literature.[26]

3.3.4 Synthesis of Methyl 7-hydroxy-2-oxo-2H-1-bensopyran-3-carboxylate (36)

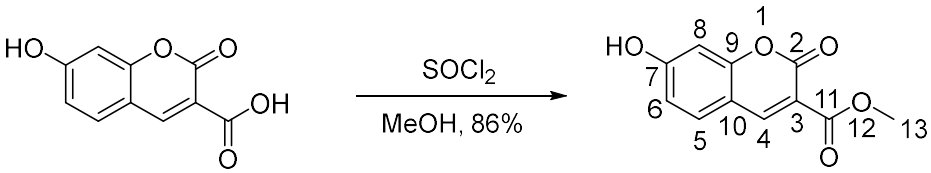

7-Hydroxycoumarin-3-carboxylic acid (0.100 g, 0.485 mmol) was dissolved in dry methanol (7 mL). This was cooled on ice before thionyl chloride (0.700 mL, 9.70 mmol) was added dropwise. The reaction was stirred on ice overnight. Sodium bicarbonate was used to neutralise the solution. The product was extracted using ethyl acetate and dried over magnesium sulphate. A grey/white solid was obtained (0.0858 g, 0.390 mmol, 86% yield).

δ_H (400 MHz, $(CD_3)_2SO$) 3.80 (3H, s, 13-H), 6.73 (1H, d, *J* = 2.2 Hz, 8-H), 6.87 (1H, dd, *J* = 8.6, 2.3 Hz, 6-H), 7.76 (1H, d, *J* = 8.61 Hz, 5-H), 8.70 (1H, s, 4-H).

δ_C (100 MHz, $(CD_3)_2SO$) 52.3 (CH_3, C13), 102.0 (CH, C8), 111.0 (C-quat, C7), 112.1 (C-quat, C9), 114.5 (CH, C6), 132.5 (CH, C5), 150.4 (CH, 4), 156.4 (C-quat, C3), 157.8 (C-quat, C10), 164.0 (C-quat, C2 or C11), 164.5 (C-quat, C2 or C11).

The NMR data reported above is comparable with that reported in the literature.[27]

3.3.5 Synthesis of Methyl 7-(dodecyloxy)-2-oxo-2H-1-benzopyran-3-carboxylate (37)

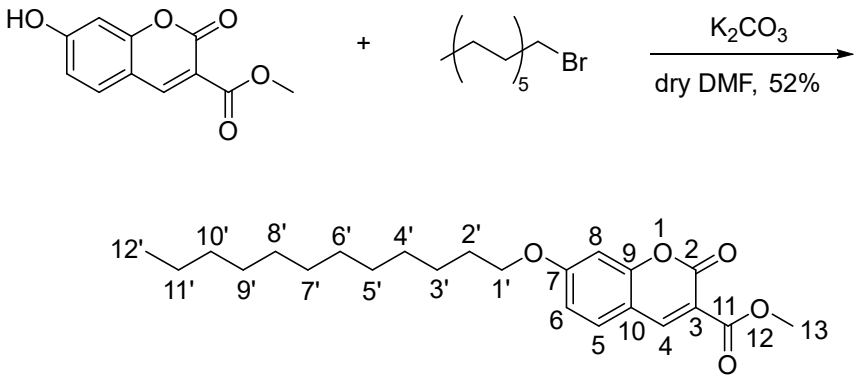

Coumarin **36** (0.0858 g, 0.416 mmol), 1-bromododecane (0.124 g, 0.499 mmol) and potassium carbonate (0.287 g, 2.08 mmol) were dissolved in dry DMF. The reaction was stirred at 60 °C overnight. Water and 6M HCl were added to neutralised the solution. The product was extracted using ethyl acetate, washed with water and dried over magnesium sulphate. This was purified via flash chromatography initial using hexane to remove the side chain then changing to 3:1 hexane/ethyl acetate. The product was obtained as a white solid (0.0775 g, 0.215 mmol, 52% yield).

δ_H (400 MHz, $CDCl_3$) 0.88 (3H, t, *J* = 7.1 Hz, 12'-H), 1.26 (15H, s, 4' to 11'-H), 1.41-1.51 (2H, m, 3'-H), 1.78-1.86 (2H, m, 2'-H), 3.94 (3H, s, 13-H), 4.04 (2H, t, *J* = 6.5 Hz, 1'-H), 6.80 (1H, d, *J* = 2.4 Hz, 8-H), 6.88 (1H, dd, *J* = 8.7, 2.3 Hz, 6-H), 7.49 (1H, d, *J* = 8.7 Hz, 5-H), 8.54 (1H, s, 4-H)

δc (100 MHz, $CDCl_3$) 14.1 (CH_3, C12'), 22.7 (alkyl CH_2), 25.9 (CH_2, C3'), 28.9 (CH_2, C2'), 29.3 (alkyl CH_2), 29.3 (alkyl CH_2), 29.5 (alkyl CH_2), 29.6 (alkyl CH_2), 29.6 (alkyl CH_2), 29.6 (alkyl CH_2), 31.9 (alkyl CH_2), 52.7 (CH_3, C13), 69.0 (CH_2, C1'), 100.8 (CH, C8), 111.5 (C-quat, C7), 113.5 (C-quat, C9), 114.1 (CH, C6), 130.7 (CH, C5), 149.6 (CH, C4), 157.3 (C-quat, C3), 157.7 (C-quat, C10), 164.2 (C-quat, C2 or C11), 164.9 (C-quat, C2 or C11).

IR vmax(film)/cm-1: 2951, 2917, 2846, 1755, 1691, 1620, 1557, 1376, 1310, 1227.

HRMS found (ESI): $[M+H]^+$, 389.2316, $C_{23}H_{33}O_5$ requires 389.2323.

3.3.6 Synthesis of 7-(dodecyloxy)-2-oxo-2H-1-benzopyran-3-carboxylic acid (38)

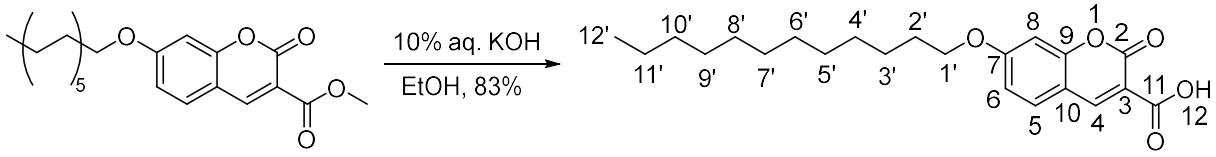

37 (0.102 g, 0.284 mmol) was dissolved in ethanol (7 mL). 10% aq. KOH solution was added (13 mL). The flask was refluxed as 80 °C for 30 minutes. Cold 6 M HCl was added under ice cold conditions to form a precipitate. This was filtered and washed with water. The product was obtained as a white solid (0.0816 g, 0.236 mmol, 83%).

δH (400 MHz, $CDCl_3$) 0.81 (3H, t, *J* = 6.7 Hz, 12'-H), 1.19 (16H, s, 4' to 11'-H), 1.35-1.47 (2H, m, 3'-H), 1.73-1.82 (2H, m, 2'-H), 4.02 (2H, t, *J* = 6.6 Hz, 1'-H), 6.84 (1H, d, *J* = 2.3 Hz, 8-H), 6.93 (1H, dd, *J* = 8.8, 2.4 Hz, 6-H), 7.56 (1H, d, *J* = 8.9 Hz, 5-H), 8.78 (1H, s, 4-H), 12.1 (1H, s, 12-OH).

δc (100 MHz, $CDCl_3$) 14.1 (CH_3, C12'), 22.7 (alkyl CH_2), 25.9 (CH_2, C3'), 28.8 (CH_2, C2'), 29.3 (alkyl CH_2), 29.3 (alkyl CH_2), 29.5 (alkyl CH_2), 29.6 (alkyl CH_2), 29.6 (alkyl CH_2), 31.9 (alkyl CH_2), 69.4 (CH_2, C1'), 101.1 (CH, C8), 110.7 (C-quat, C2 or C11), 112.1 (C-quat, C7), 115.4 (CH, C6), 131.6 (CH, C5), 151.2 (CH, C4), 157.1 (C-quat, C10), 163.2 (C-quat, C2 or C11), 164.6 (C-quat, C3), 165.9 (C-quat, C9).

The NMR data reported above is in line with literature data.[28]

3.3.7 Synthesis of Amphiphilic Ligand 31

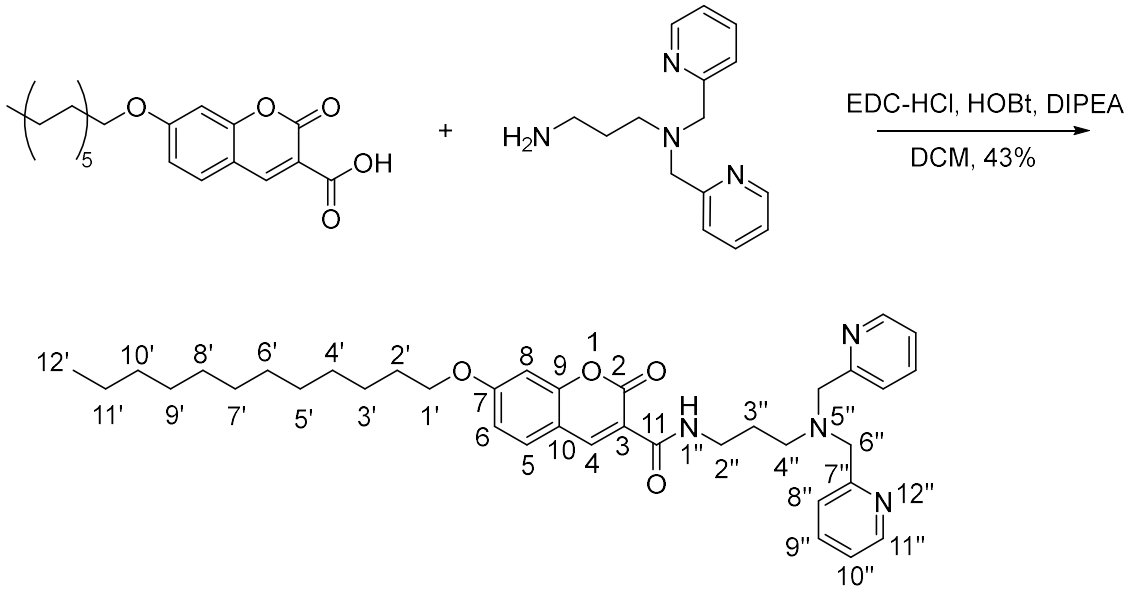

34 (0.0501 g, 0.195 mmol), **38** (0.616 g, 0.195 mmol), EDC-HCl (0.0748 g, 0.390 mmol), HOBt (0.0530 g, 0.390 mmol) and DIPEA (67.9 µL, 0.390 mmol) were dissolved in dry DCM (10 mL). The reaction was stirred at room temperature overnight. The product was extracted with DCM and washed with water. This was purified using flash chromatography on alumina starting with DCM then increasing to 2% MeOH in DCM to give the product (51.4 mg, 0.0839 mmol, 43%) as a yellow semi-solid.

δ_H (400 MHz, $CDCl_3$) 0.84 (3H, t, *J* = 6.8 Hz, 12'-H), 1.23 (15H, s, 3'-H to 15'-H), 1.38-1.49 (2H, m, 3'-H), 1.74-1.89 (4H, m, 2'-H and 3''-H), 2.62 (2H, t, *J* = 6.9 Hz, 4''-H), 3.41 (1H, d, *J* = 6.7 Hz, $2''_A$-H), 3.45 (1H, d, *J* = 6.9 Hz, $2''_B$-H), 3.80 (4H, s, 6''-H), 4.01 (2H, t, *J* = 6.5 Hz, 1'-H), 6.80 (1H, d, *J* = 2.3 Hz, 8-H), 6.88 (1H, dd, *J* = 8.6, 2.4 Hz, 6-H), 7.08 (2H, ddd, *J* = 7.5, 4.9, 1.2 Hz, 10''-H), 7.48-7.54 (3H, m, 5-H and 8''-H), 7.60 (2H, td, *J* = 7.7, 1.7 Hz, 9''-H), 8.45-8.49 (2H, m, 11''-H), 8.70 (1H, t, *J* = 5.6 Hz, 1''-NH), 8.75 (1H, s, 4-H).

δ_C (100 MHz, $CDCl_3$) 14.1 (CH_3, C12'), 22.7 (alkyl CH_2), 25.9 (CH_2, C3'), 28.8 (CH_2, C2'), 29.3 (alkyl CH_2), 29.5 (alkyl CH_2), 29.6 (alkyl CH_2), 31.9 (alkyl CH_2), 69.4 (CH_2, C1'), 101.1 (CH, C8), 110.7 (C-quat, C2 or C11), 112.1 (C-quat, C7), 115.4 (CH, C6),

131.6 (CH, C5), 151.2 (CH, C4), 157.1 (C-quat, C10), 163.2 (C-quat, C2 or C11), 164.6 (C-quat, C3), 165.9 (C-quat, C9).

IR vmax(film)/cm-1: 3346, 3043, 2920, 2849, 1705, 1598, 1532, 1469, 1368, 1220.

HRMS found (ESI): $[M+Na]^+$, 635.3548, $C_{37}H_{48}N_4NaO_4$ requires 635.3568.

3.4 Synthesis of Control Molecule 32

3.4.1 Synthesis of Coumarin 39

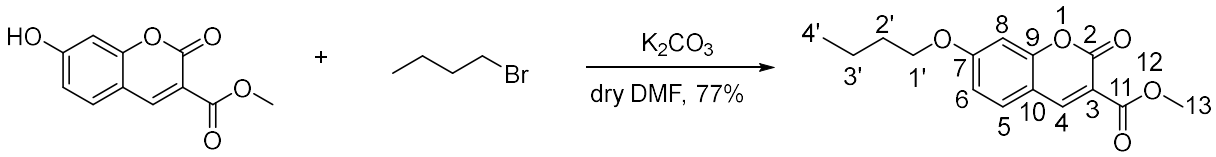

35 (0.124 g, 0.562 mmol), 1-bromobutane (0.34 mL, 0.674 mmol) and K_2CO_3 (0.388 g, 2.81 mmol) were dissolved in dry DMF and stirred overnight at 60°C. Water and 6 M HCl were added to the reaction flask to neutralise the solution. Ethyl acetate was used to extract the product into the organic layer. This was then washed with water and dried over $MgSO_4$. The product was obtained as a white solid (0.12 g, 0.434 mmol, 77%).

δ_H (400 MHz, $CDCl_3$) 0.99 (3H, t, *J* = 7.4 Hz, 4'-H), 1.45-1.56 (2H, m, 3'-H), 1.77-1.86 (2H, m, 2'-H), 3.95 (3H, s, 13-H), 4.05 (2H, t, *J* = 6.5 Hz, 1'-H), 6.80 (1H, d, 2.3 Hz, 8-H), 6.88 (1H, dd, *J* = 8.8, 2.3 Hz, 6-H), 7.49 (1H, d, *J* = 8.7 Hz, 5-H), 8.54 (1H, s, 4-H).

δ_C (100 MHz, $CDCl_3$) 13.7 (CH_3, C4'), 19.1 (CH_2, C3'), 30.9 (CH_2, C2'), 52.7 (CH_3, C13), 68.7 (CH_2, C1'), 100.8 (CH, C8), 111.5 (C-quat, C7), 113.5 (C-quat, C2 or C11), 114.1 (CH, C6), 130.8 (CH, C5), 149.5 (CH, C4), 157.2 (C-quat, C2 or C11), 157.7 (C-quat, C10), 164.2 (C-quat, C3), 164.9 (C-quat, C9).

IR vmax(film)/cm-1: 3050, 2953, 2870, 1736, 1691, 1592, 1554, 1375, 1375, 1216.

HRMS found (ESI): $[M+Na]^+$, 299.0886, $C_{15}H_{16}NaO_5$ requires 299.0890.

3.4.2 Synthesis of 7-butoxy-2-oxo-2H-1-benzopyran-3-carboxylic acid (40)

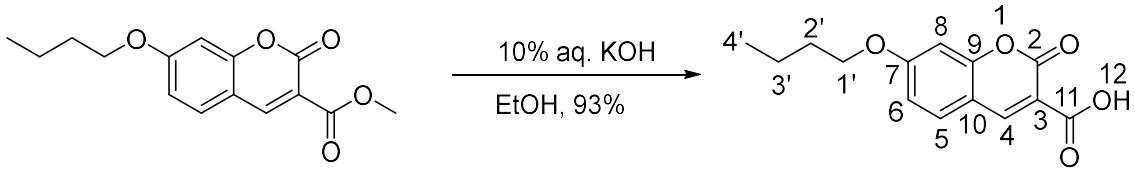

38 (0.12 g, 0.434 mmol) was dissolved in ethanol (7 mL). 10% aq. KOH solution was added (13 mL). The flask was refluxed as 80°C for 30 minutes. Cold 6M HCl was added under ice cold conditions to form a precipitate. This was filtered and washed with water. The product was obtained as a white solid (0.105 g, 0.399 mmol, 93%).

δ_H (400 MHz, $CDCl_3$) 0.99 (3H, t, *J* = 7.7 Hz, 4'-H), 1.78-1.87 (2H, m, 2'-H), 4.09 (2H, t, *J* = 6.4 Hz, 1'-H), 6.90 (1H, d, *J* = 2.3 Hz, 8-H), 6.99 (1H, dd, *J* = 8.7, 2.3, 6-H), 7.61 (1H, d, *J* = 8.8 Hz, 5-H), 8.84 (1H, s, 4-H), 12.13 (1H, s, 12-H).

δ_C (100 MHz, $CDCl_3$) 13.7 (CH_3, C4'), 19.1 (CH_2, C3'), 30.8 (CH_2, C2'), 69.1 (CH_2, C1'), 101.2 (CH, C8), 110.7 (C-quat, C7), 112.2 (C-quat, C2), 115.5 (CH, C6), 131.7 (CH, C5), 151.2 (CH, C4), 157.1 (C-quat, C10), 163.2 (C-quat, C11), 164.6 (C-quat, C3), 165.9 (C-quat, C9).

IR vmax(film)/cm-1: 3050, 2955, 2921, 2872, 1735, 1681, 1600, 1502, 1383, 1254.

HRMS found (ESI): $[M+H]^+$, 263.0905, $C_{14}H_{15}O_5$ requires 263.0914.

3.4.3 Synthesis of Control Molecule 32

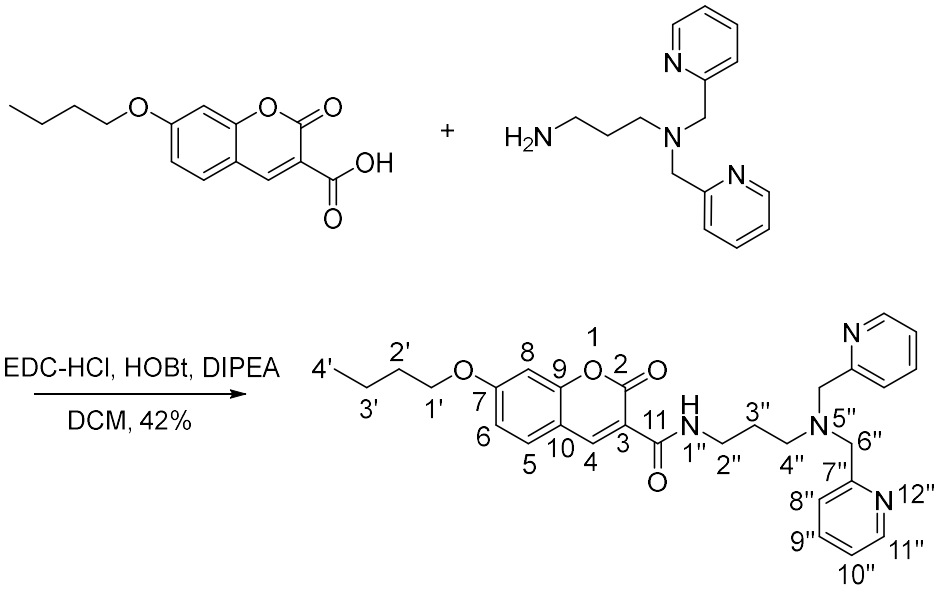

To a solution of **34** (0.099 g, 0.386 mmol) in dry DCM the following was added, **40** (0.101 g, 0.386 mmol), EDC-HCl (0.148 g, 0.772 mmol), HOBt (0.104 g, 0.772 mmol), DIPEA (0.0997 g, 0.772 mmol). This was stirred at room temperature overnight. The product was extracted with DCM and washed with water. It was purified using flash chromatography on alumina. Starting with DCM until the top spot starts coming off, then increase to 1% MeOH/DCM then to 5% MeOH/DCM. The product was obtained as a yellow oil (0.080 g, 0.160 mmol, 42%).

δ_H (400 MHz, $CDCl_3$) 0.90 (3H, t, *J* = 7.5 Hz, 4'-H), 1.36-1.48 (2H, m, 3'-H), 1.67-1.75 (2H, m, 3''-H), 1.75-1.83 (2H, m, 2'-H), 2.57 (2H, t, *J* = 6.9 Hz, 4''-H), 3.36 (1H, d, *J* = 6.7 Hz, $2''_A$-H), 3.40 (1H, d, *J* = 6.7 Hz, $2''_B$-H), 3.75 (4H, s, 6''-H), 3.96 (2H, t, *J* = 6.5 Hz, 1'-H), 6.74 (1H, d, *J* = 2.1 Hz, 8-H), 6.82 (1H, dd, *J* = 8.8, 2.4 Hz, 6-H), 7.03 (2H, t, *J* = 6.1 Hz, 10''-H), 7.43-7.48 (3H, m, 5-H and 8''-H), 7.55 (2H, td, *J* = 7.6, 1.8 Hz, 9''-H), 8.41 (2H, d, *J* = 4.2 Hz, 11''-H), 8.65 (1H, t, *J* = 5.5 Hz, 1''-H), 8.70 (1H, s, 4-H).

δ_C (100 MHz, $CDCl_3$) 13.5 (CH_3, C4'), 19.1 (CH_2, C3'), 26.9 (CH_2, C2'), 30.9 (CH_2, C3''), 37.8 (CH_2, C2''), 51.7 (CH_2, C4''), 60.4 (CH_2, C6''), 68.7 (CH_2, C1'), 100.6 (CH, C8), 112.1 (C-quat, C7), 114.3 (CH, C6), 114.6 (C-quat, C9), 121.8 (CH, C10), 123.1 (CH, C8''), 130.9 (CH, C5), 136.4 (CH, C9''), 147.9 (CH, C4), 148.9 (CH, C11''), 156.6 (C-

quart, C10), 159.6 (C-quat, C7''), 161.7 (C-quat, C2 or C11), 161.9 (C-quat, C3), 164.3 (C-quat, C2 or C11)

IR vmax(film)/cm-1: 3366, 3046, 2930, 2870, 2813, 1713, 1592, 1524, 1370, 1221.

HRMS found (ESI): $[M+Na]^+$, 523.2314, $C_{29}H_{32}N_4NaO_4$ requires 523.2316

References

1. Liu, X.; Ngo, H. T.; Ge, Z.; Butler, S. J.; Jolliffe, K. A., Tuning colourimetric indicator displacement assays for naked-eye sensing of pyrophosphate in aqueous media. *Chemical Science* **2013,** *4* (4), 1680-1686.
2. Wu, D.; Sedgwick, A. C.; Gunnlaugsson, T.; Akkaya, E. U.; Yoon, J.; James, T. D., Fluorescent chemosensors: the past, present and future. *Chemical Society Reviews* **2017,** *46* (23), 7105-7123.
3. Jolliffe, K. A., Pyrophosphate recognition and sensing in water using bis [zinc (II) dipicolylamino]-functionalized peptides. *Accounts of chemical research* **2017,** *50* (9), 2254-2263.
4. Robinson, G. A.; Butcher, R. W.; Sutherland, E. W., cyclic AMP. *Annual review of biochemistry* **1968,** *37* (1), 149-174.
5. Nguyen, B. T.; Anslyn, E. V., Indicator–displacement assays. *Coordination chemistry reviews* **2006,** *250* (23-24), 3118-3127.
6. Sedgwick, A. C.; Brewster, J. T.; Wu, T.; Feng, X.; Bull, S. D.; Qian, X.; Sessler, J. L.; James, T. D.; Anslyn, E. V.; Sun, X., Indicator displacement assays (IDAs): the past, present and future. *Chemical Society Reviews* **2021**.
7. Sousa, L. R.; Larson, J. M., Crown ether model systems for the study of photoexcited state response to geometrically oriented perturbers. The effect of alkali metal ions on emission from naphthalene derivatives. *Journal of the American Chemical Society* **1977,** *99* (1), 307-310.
8. Hanshaw, R. G.; Hilkert, S. M.; Jiang, H.; Smith, B. D., An indicator displacement system for fluorescent detection of phosphate oxyanions under physiological conditions. *Tetrahedron letters* **2004,** *45* (47), 8721-8724.
9. Nie, S.; Xing, Y.; Kim, G. J.; Simons, J. W., Nanotechnology applications in cancer. *Annu. Rev. Biomed. Eng.* **2007,** *9*, 257-288.
10. Joshi, M.; Bhattacharyya, A.; Ali, S. W., Characterization techniques for nanotechnology applications in textiles. **2008**.
11. Ren, C. Z. J.; Solis-Munana, P.; Warr, G. G.; Chen, J. L. Y., Dynamic and modular formation of a synergistic transphosphorylation catalyst. *ACS Catalysis* **2020,** *10* (15), 8395-8401.

12. Solís-Muñana, P.; Salam, J.; Ren, C. Z. J.; Carr, B.; Whitten, A. E.; Warr, G. G.; Chen, J. L. Y., An Amphiphilic (salen) Co Complex–Utilizing Hydrophobic Interactions to Enhance the Efficiency of a Cooperative Catalyst. *Advanced Synthesis & Catalysis* **2021,** *363* (13), 3207-3213.
13. Ren, C. Z. J.; Solís Muñana, P.; Dupont, J.; Zhou, S. S.; Chen, J. L. Y., Reversible Formation of a Light-Responsive Catalyst by Utilizing Intermolecular Cooperative Effects. *Angewandte Chemie* **2019,** *131* (43), 15398-15402.
14. Ngo, H. T.; Liu, X.; Jolliffe, K. A., Anion recognition and sensing with Zn (II)–dipicolylamine complexes. *Chemical Society Reviews* **2012,** *41* (14), 4928-4965.
15. Greenberg, J. A.; Sammakia, T., The conversion of tert-butyl esters to acid chlorides using thionyl chloride. *The Journal of organic chemistry* **2017,** *82* (6), 3245-3251.
16. Yearty, K. L.; Maynard, R. K.; Cortes, C. N.; Morrison, R. W., A multioutcome experiment for the Williamson ether synthesis. *Journal of Chemical Education* **2020,** *97* (2), 578-581.
17. Valeur, E.; Bradley, M., Amide bond formation: beyond the myth of coupling reagents. *Chemical Society Reviews* **2009,** *38* (2), 606-631.
18. Valizadeh, H.; Gholipur, H.; Shockravi, A., Microwave assisted synthesis of coumarins via potassium carbonate catalyzed knoevenagel condensation in 1-n-butyl-3-methylimidazolium bromide ionic liquid. *Journal of heterocyclic chemistry* **2007,** *44* (4), 867-870.
19. Bečić, E.; Šober, M.; Imamović, B.; Završnik, D.; Špirtović-Halilović, S., UV/VIS absorption and fluorescence spectroscopic study of some 3-substituted derivatives of 4-hydroxycoumarin. *Pigment & Resin Technology* **2011**.
20. Liu, X.; Cole, J. M.; Low, K. S., Solvent effects on the UV–vis absorption and emission of optoelectronic coumarins: a comparison of three empirical solvatochromic models. *The Journal of Physical Chemistry C* **2013,** *117* (28), 14731-14741.
21. Nigam, S.; Rutan, S., Principles and applications of solvatochromism. *Applied Spectroscopy* **2001,** *55* (11), 362A-370A.

22. Fonge, H.; Jin, L.; Cleynhens, J.; Bormans, G.; Verbruggen, A., 99mTc-tricarbonyl labeled agents for cell labeling: Development, biodistribution in normal mice and preliminary in vitro evaluation. *Bioorganic & medicinal chemistry* **2010,** *18* (1), 396-402.
23. Feng, R.; Xu, Y.; Zhao, H.; Duan, X.; Sun, S., A novel platform self-assembled from squaraine-embedded Zn (ii) complexes for selective monitoring of ATP and its level fluctuation in mitotic cells. *Analyst* **2016,** *141* (11), 3219-3223.
24. Mambanda, A.; Jaganyi, D., Understanding the role of the flexible bridging linker through kinetics and mechanistic study of Pt (II) amphiphiles derived from a bis (2-pyridylmethyl) amine chelate head group. *Dalton Transactions* **2011,** *40* (1), 79-91.
25. Kambam, S.; Ren, X.; Zheng, C.; Wang, F.; Wang, Y.; Chen, H.; Yin, J.; Xie, J.; Chen, X., The synthesis of UDP-selective fluorescent probe and its imaging application in living cells. *Bioorganic & medicinal chemistry letters* **2015,** *25* (2), 262-265.
26. Darvatkar, N. B.; Deorukhkar, A. R.; Bhilare, S. V.; Raut, D. G.; Salunkhe, M. M., Ionic liquid–mediated synthesis of coumarin-3-carboxylic acids via knoevenagel condensation of meldrum's acid with ortho-hydroxyaryl aldehydes. *Synthetic Communications*® **2008,** *38* (20), 3508-3513.
27. Valizadeh, H.; Vaghefi, S., One-pot Wittig and Knoevenagel reactions in ionic liquid as convenient methods for the synthesis of coumarin derivatives. *Synthetic Communications*® **2009,** *39* (9), 1666-1678.
28. Gruber, B.; Stadlbauer, S.; Woinaroschy, K.; König, B., Luminescent vesicular receptors for the recognition of biologically important phosphate species. *Organic & biomolecular chemistry* **2010,** *8* (16), 3704-3714.

Appendices

Hexadecyl bis(2-pyridylmethyl)amine (29)

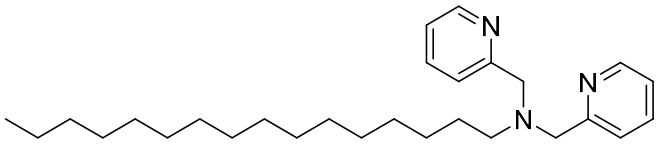

^{1}H NMR

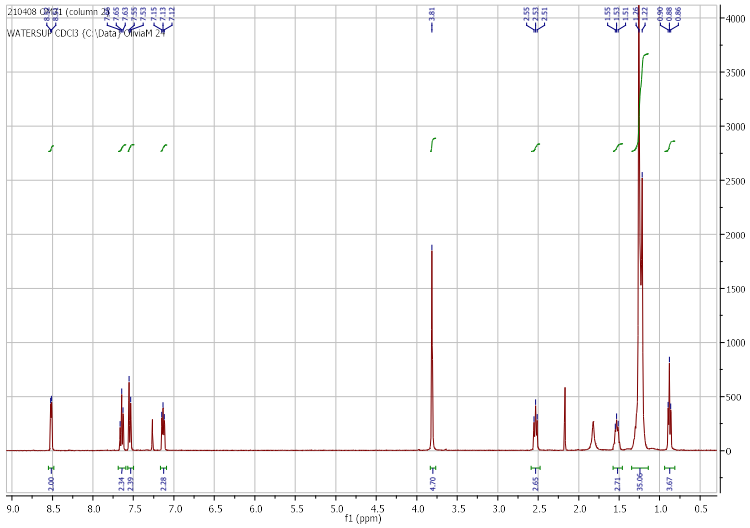

^{13}C NMR

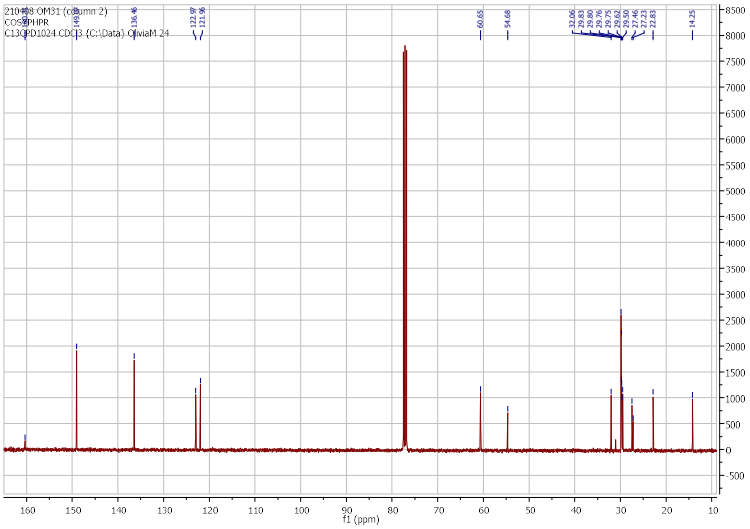

Methyl 7-(dodecyloxy)-2-oxo-2H-1-benzopyran-3-carboxylate (37)

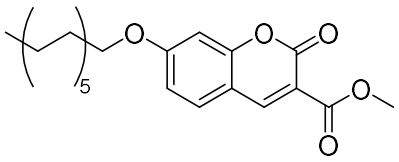

^{1}H NMR

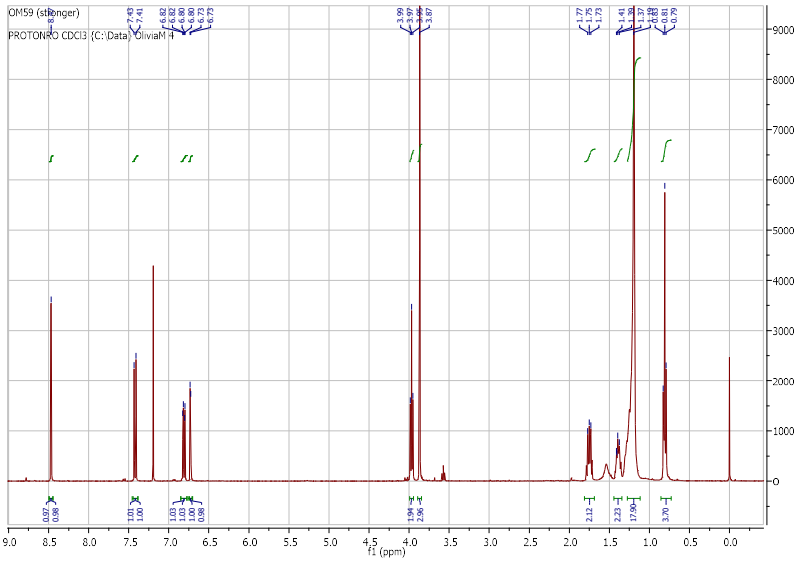

^{13}C NMR

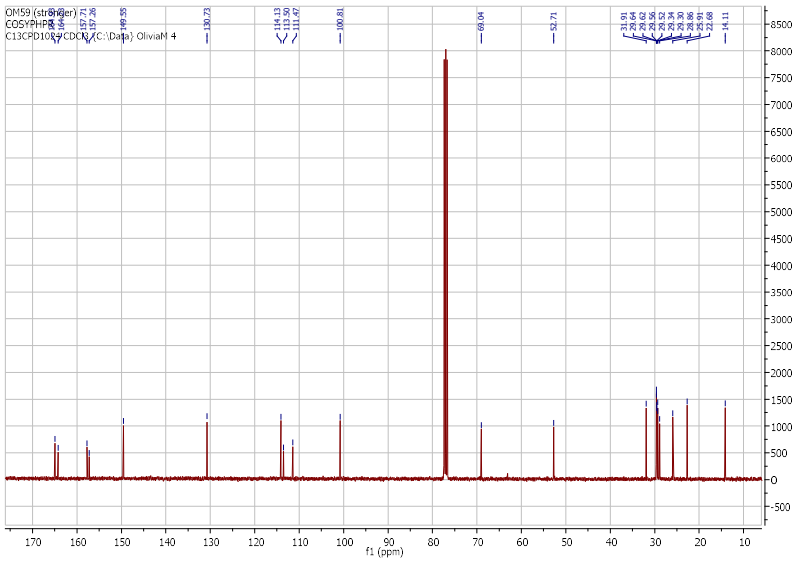

Sensor 31

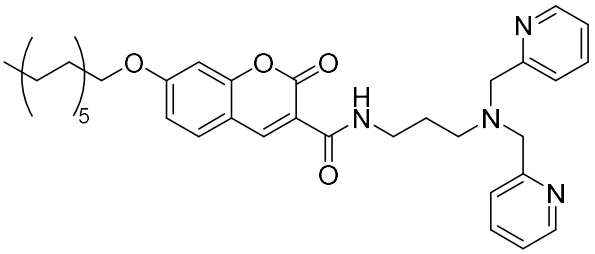

^{1}H NMR

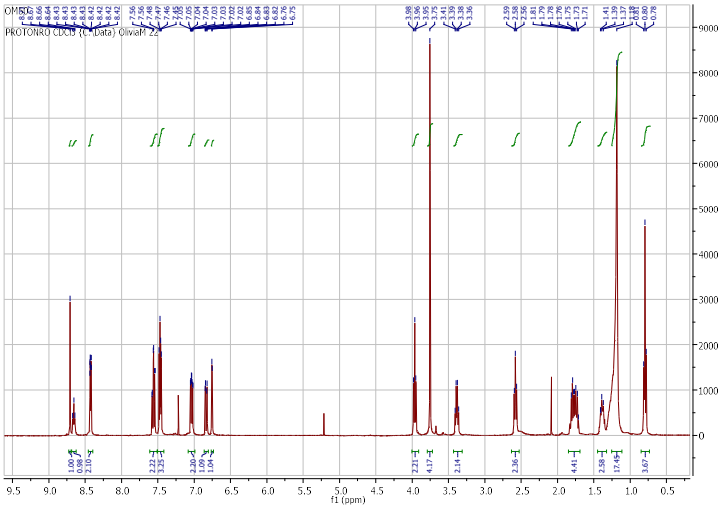

^{13}C NMR

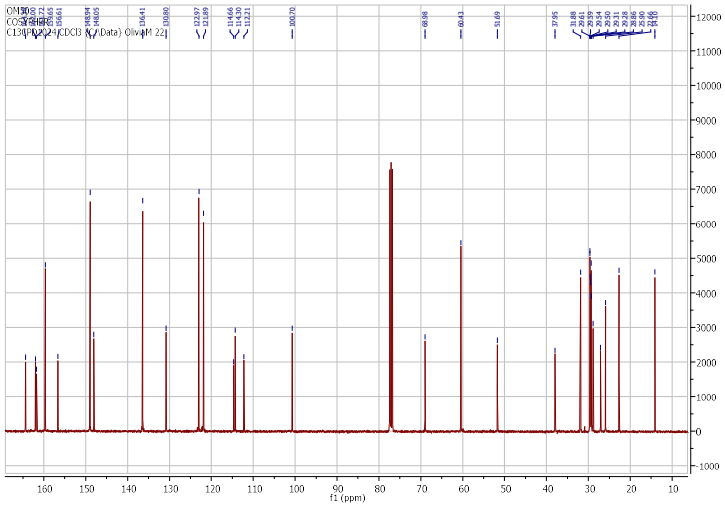

Coumarin 39

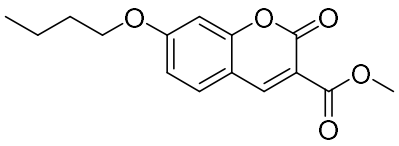

^{1}H NMR

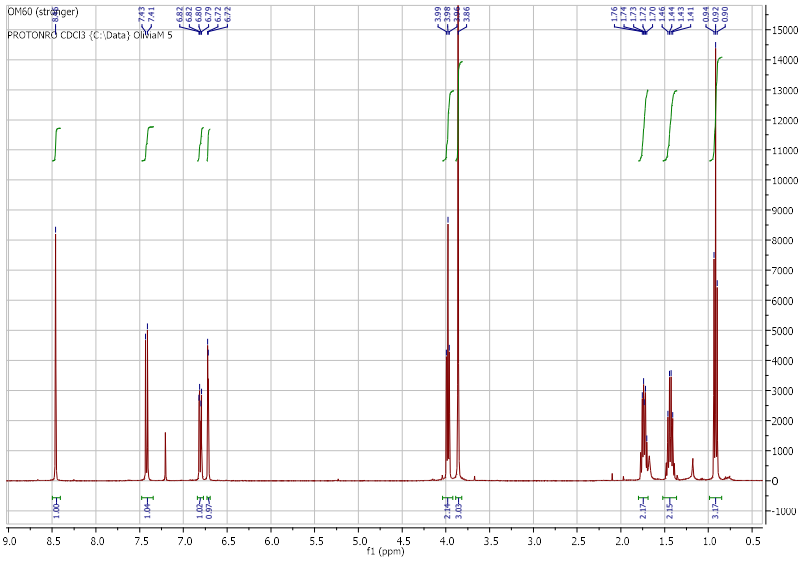

^{13}C NMR

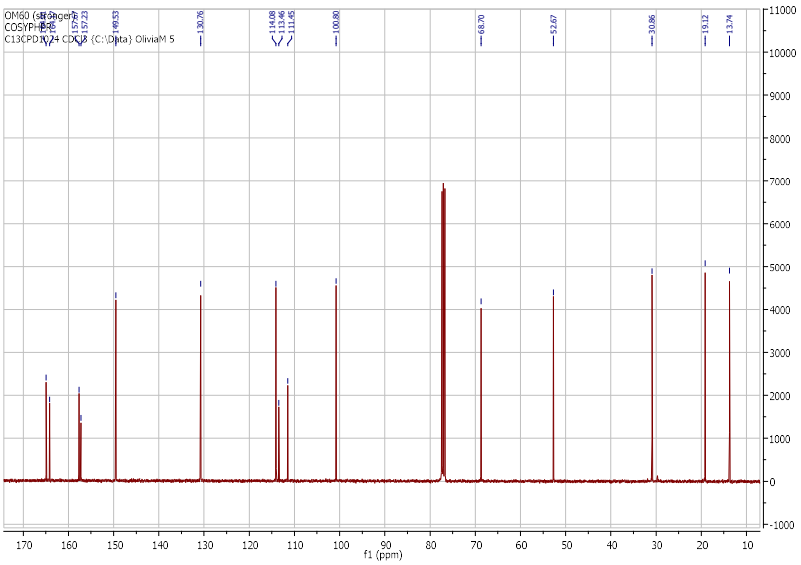

7-butoxy-2-oxo-2H-1-benzopyran-3-carboxylic acid (40)

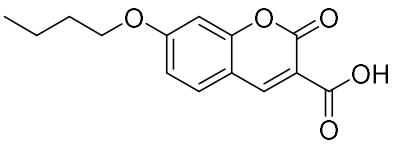

^{1}H NMR

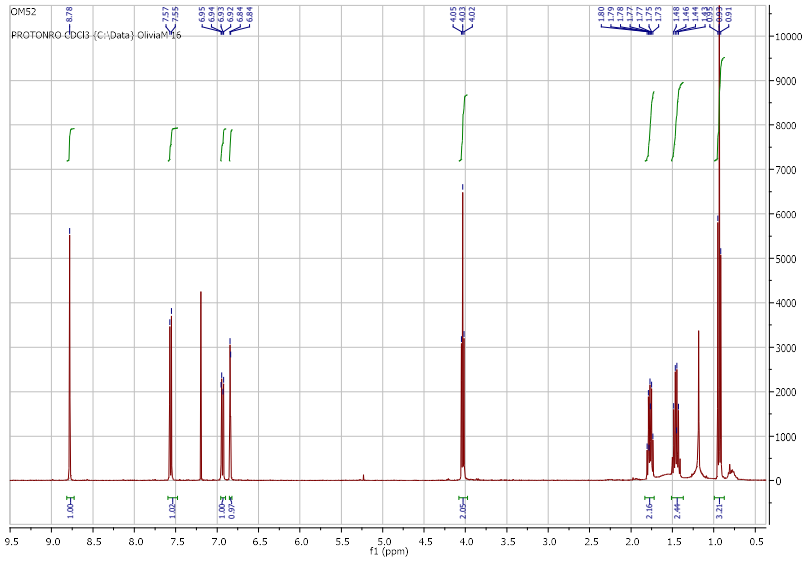

^{13}C NMR

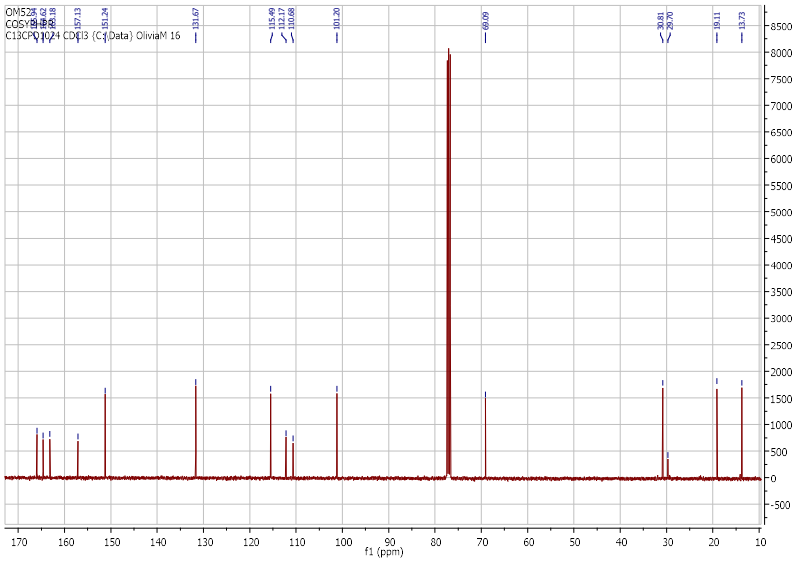

Sensor 32

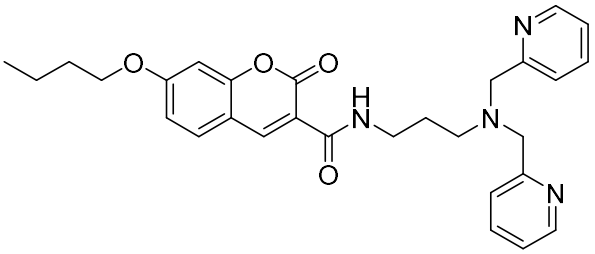

^{1}H NMR

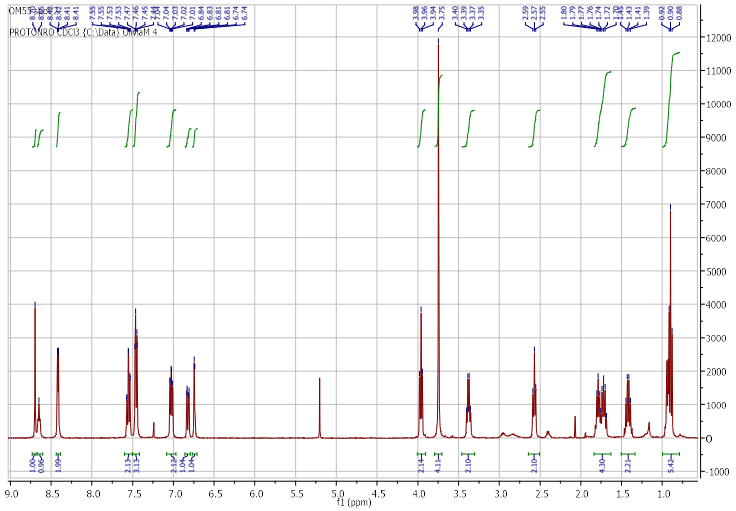

^{13}C NMR